

Instrumentation Prospects for Rocky Exoplanet Atmospheres Studies with High Resolution Spectroscopy

Surangkhan Rukdee^{1,*}

¹Max Planck Institute for Extraterrestrial Physics, Giessenbachstrasse, 85748 Garching, Germany

*suri@mpe.mpg.de

ABSTRACT

Studying the atmospheres of exoplanets is one of the most promising ways to learn about distant worlds beyond our solar system. The composition of an exoplanet's atmosphere can provide critical insights into its geology and potential habitability. For instance, the presence of certain molecules such as water vapor, oxygen, or methane have been proposed to indicate the possibility of life. From an observation point of view, over the past fifteen years, significant progress has been made in characterizing exoplanetary atmospheres. This work reviews recent developments in ground-based high-resolution spectroscopic instruments that make it possible to analyze distant atmospheres in great detail. High-resolution transmission spectroscopy, one of the most effective methods used, has examined the atmospheres of Jupiter-like and is pushing towards the smaller, sub-Neptunian exoplanets. Numerous molecules have been detected using this technique, including CO, H₂O, TiO, HCN, CH₄, NH₃, C₂H₂, OH. We explore the intriguing possibilities that lie ahead for future ground-based instrumentation, particularly in the context of detecting biologically relevant molecules within Earth-analog exoplanetary atmospheres including molecular oxygen (O₂). With detailed exposure time calculations for detecting O₂ we find that at the same exposure time spectral resolution of 300,000 reaches higher significance compared to 100,000. The exposure time and therefore the needed number of transits is reduced by a factor of 4 in challenging haze and cloud scenarios.

1 Introduction

Instrumentation has played a pivotal role in exoplanetary research over the last thirty years. Before 1995, our understanding of exoplanets primarily relied on philosophical and theoretical considerations¹. Technical developments opened the possibility to detect and characterize exoplanets. Now, one of the most minute features in the cosmos, the thin atmospheres wrapped around distant exoplanets are being measured both from ground-based and space-based instruments. Observing the atmospheres around rocky planets, also known as terrestrial exoplanets, poses a significant technical challenge in the next decades.

1.1 State of the art in instrumentation for exoplanet atmosphere studies

Observing exoplanet atmospheres presents several difficult challenges². Directly seeing the emitted spectrum of exoplanets or their atmospheres is challenging due to the glare of their host stars. The star outshines the faint exoplanets with the contrast ranging from 10^{-3} to 10^{-10} for hot Jupiters to Earth-Sun analogs. Contrast, the brightness ratio between an astronomical source such as a planet and the star it orbits, is key for direct imaging. The ratio $\frac{F_{\text{source}}}{F_{\text{Star}}}$ is small indicating the source (planet) is much fainter than the star³. Moreover, exoplanets are often located at orbital distances of sub-arcsecond from their host stars, making a spatial separation of the light, for example with coronagraphs, difficult. Direct imaging is most sensitive to planets orbiting at distances greater than 5 AU from their host stars⁴. In Figure 1, current directly imaged planets are shown as red squares, typically of planets of thousand times the mass of Earth. This technique enables the direct recording of photons emitted by these planets, facilitating their spectroscopic or photometric characterization. This has led to the discovery of Jupiter analogs such as 51 Eri b⁵ and AF Lep b⁶, which are inaccessible to transit spectroscopy because their orbits are not passing in front of the host star from our point of view. The High Contrast Imaging (HCI) reflected light observation is often aided by high-contrast systems⁷, which is a combination of Extreme Adaptive Optic (ExAO) systems, coronagraphs, wavefront sensing, differential imaging techniques³ and integral field spectrographs. The ExAO⁸ helps to remove most of the optical aberrations induced by atmospheric turbulence and perform fine wavefront correction such as GPI^{9,10}, SCExAO¹¹, and SPHERE¹². The internal coronagraph applies design masks and optical components inside the telescope to induce starlight destructive interference at the expected location of a planet in the image with Lyot mask¹³ or Pupil Apodization^{14–17}. The sensitivity of high-contrast imaging can be limited by speckles making diffracted starlight at the position of the planet. Speckles originate from atmospheric turbulence and optical aberrations within the instruments¹⁸. Including an integral field spectrograph helps remove speckles and

acquire spectra, such as P1640+Palm3000¹⁹. The Subaru Coronagraphic Extreme Adaptive Optics (SCExAO) has achieved high-quality adaptive optics corrections with a Strehl ratio of $\sim 90\%$ at $1.6 \mu\text{m}$ under favorable conditions, attaining planet-to-star contrasts of $(\sim 10^{-6}$ at $0.5''$)²⁰, comparable to those achieved by GPI⁵ and SPHERE²¹. SCExAO has also reached extreme AO-like contrasts for stars as faint as 12th magnitude in the optical.

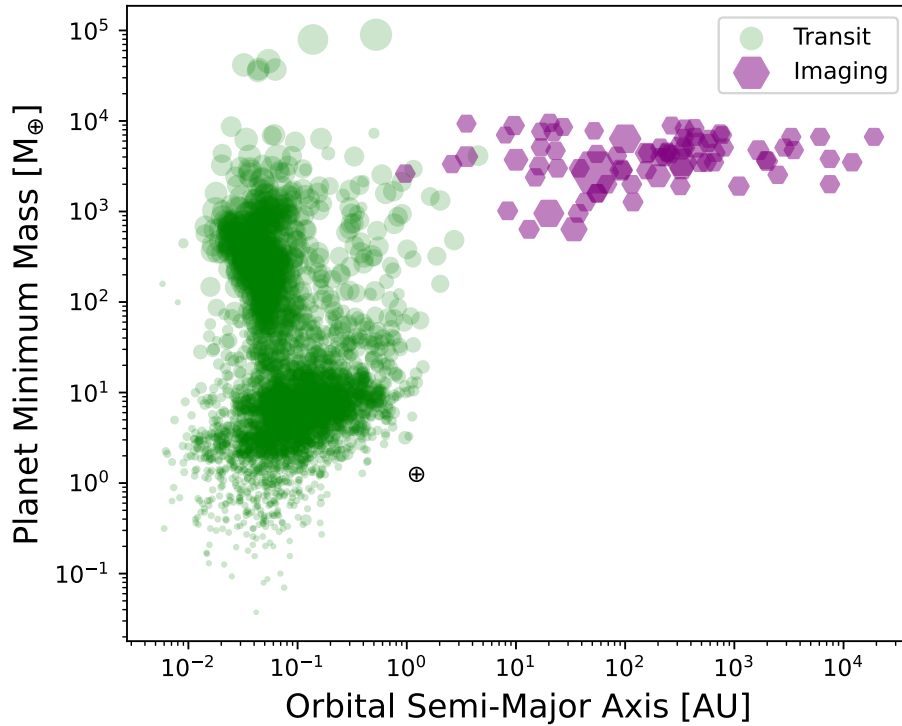


Figure 1. The confirmed exoplanets discovered with high-contrast imaging (purple) are compared to those found with transits (green) as of September 2024 from the NASA Exoplanet Archive. The marker size corresponds to the relative radius.

Molecule detection can be enhanced by high-resolution spectroscopy. Two decades ago, high dispersion spectroscopy (HDS) was suggested^{22,23} as a way to boost detection capabilities by relying on the numerous spectral features expected in the spectra of exoplanets. Utilizing a high-resolution spectrograph can remove speckles by applying a high-pass filter while keeping the molecular signatures of the planet spectrum nearly intact¹⁸. One of the most recent developments in high-contrast imaging for studying exoplanet atmospheres includes the incorporation of a high-resolution spectrograph in a scheme known as high-dispersion coronagraphy (HDC) to achieve a contrast of up to 10^{-7} ²⁴. HDC was first coined with an experiment²⁵, which demonstrated that it could achieve contrasts exceeding 10^{-7} , depending on the target and whether observations are conducted from space or the ground. Projects employing HDC include HiRISE at VLT (combining SPHERE and CRIRES)²⁶, Subaru/REACH²⁷, and the Keck Planet Imager and Characterizer (KPIC)²⁸ at Keck. Recent results show that they are suitable for giant planets^{26,29}.

Looking into the future, the combination of SPHERE and ESPRESSO^{30,31} is expected to observe O₂ around Proxima b atmosphere within 60 nights at the Very Large Telescope (VLT) assuming a total system transmission budget of 3 – 4%. One challenge in observing Proxima b is the star-planet separation of $0.03''$, although this subarcsecond measurement can be achieved with an instrument similar to GRAVITY³², the H-band instrument offers an efficiency of 1-2%³³. The current limitation of GRAVITY will be overcome with GRAVITY+, which will enhance the detection capability of exoplanets in the J and K bands. Looking into the future, a previous study³⁴ cautions that with a 39-meter Extremely Large Telescope (ELT), in the case of studying the α Centauri AB system with high-contrast imaging, a separation of $\sim 1''$ would correspond to $\sim 17.5\lambda/D$ and would therefore likely be close to background-limited. The first-generation ELT spectrograph HARMONI³⁵ is expected to reach a contrast of a few 10^{-7} at 50 mas for bright targets in a photon noise regime with molecular mapping³⁶ in the range of $1.45\text{--}2.45 \mu\text{m}$ at $R=18,000$. With this resolution, a recent simulation for Proxima b³⁷ shows that the measured spectrum is expected to be dominated by tellurics and the stellar continuum. Secondly, the first-generation ELT spectrograph METIS³⁸ combines high-resolution spectroscopy and high-contrast imaging. It will offer a unique capacity to characterize exoplanet atmospheres in the L and M bands, $3\text{--}5 \mu\text{m}$ range with a spectral resolution of with $R=100,000$ in integral field unit (IFU) mode.

Further into the future, the second generation high-resolution spectrograph ANDES³⁹, the 2nd generation instrument of the E-ELT, will unlock observations of terrestrial exoplanet atmospheres with high contrast and high-resolution techniques⁴⁰.

Today, the most common method used to investigate exoplanet atmospheres involves transit spectroscopy. Transmission spectroscopy is most effective for close-in planets, as the probability and frequency of transit events decrease significantly with orbital distance⁴¹. In contrast, observations of reflected light spectra allow atmospheric characterization of planets at larger orbital separations, offering complementary insights to those obtained through transmission spectroscopy⁴². A challenge here is the alignment of the system so that it passes in front or behind its host star along our line of sight, known as a transit or secondary eclipse. Furthermore, the planet orbital period constrains the observing cadence by which more transit spectra can be obtained. Spectra acquired during transits can give clues on the chemical composition of exoplanet atmospheres^{43,44}. As a planet crosses the observer's line of sight to the host star, atmospheric molecules produce distinctive spectral features through absorption lines. With the transmission spectroscopy technique, the most crucial factors are the duration and the planetary radius or atmosphere height relative to the host star radius, which sets the brightness decrease. Since timing is critical for transit studies, maximizing signal acquisition within a single transit is crucial.

High-resolution ($R = 25,000 - 100,000$)² observations improve reliability by better disentangling overlapping telluric features and concentrating spectral peaks on a few resolution elements while spreading background noise. Ground-based transit spectroscopy involves atmospheric absorption features from Earth's atmosphere (telluric features), posing the challenge of distinguishing them from extraterrestrial features. Higher resolution capabilities, ideally $R \sim 100,000$ ¹, are crucial for secure and efficient identification of complex spectral features, especially in separating overlapping absorption features from different molecules. Each detected line using the high-resolution technique enhances the overall planet signal-to-noise ratio by number of lines² within the spectral features or band (Equation 1). The planet signal to noise ratio (SNR) is described in previous study⁴⁵ as:

$$SNR_p = \frac{S_p}{S_*} \times SNR_* \times \sqrt{N_{lines}} \quad (1)$$

where SNR_p is the signal-to-noise ratio of the planet, where S_p represents the planet's signal, S_* denotes the stellar signal, and N_{lines} refers to the number of lines within the spectral feature.

Increasing spectral resolution from $R=100,000$ to $R=300,000$ roughly doubles average line depth⁴⁶ and could potentially reduce the number of transits needed for a 3σ detection of O_2 around terrestrial exoplanets by up to 35%⁴⁶⁻⁴⁸. This technique was proposed to be conducted with G-CLEF⁴⁹ spectrograph at GMT with the assistance of the resolution booster^{48,50}. With both HCI and transmission spectroscopy techniques mentioned above, high spectral resolutions enhance detection capabilities for studying exoplanets and their atmospheres.

1.2 High-resolution atmosphere observations

In the last decade, the High-Resolution Spectroscopy (HRS) technique has empowered astronomers to detect minute features on the surface of exoplanets. These include determining the velocity of winds⁵¹ traversing the terminator regions of exoplanets, investigating phenomena such as thermal inversion layers and escape processes⁵²⁻⁵⁴, and unveiling critical information about the orbital inclinations and rotations of various exoplanets^{55,56}. Moreover, high-resolution spectroscopy has enabled the identification of molecular and atomic species within the atmospheres of diverse exoplanets⁵⁷⁻⁵⁹ and detailed measurements of isotopologues⁶⁰. Precise measurements of chemical abundance can pinpoint where within the protoplanetary disk, the planets were formed^{61,62}.

The ground-based study of exoplanet atmospheres started with the groundbreaking detection of sodium (Na) around the atmosphere of HD209458b⁴⁴. In 2010, another significant milestone was reached when carbon monoxide (CO) was identified in the same planetary atmosphere⁵², marking the start of a popular observational technique known as High-Resolution Cross-Correlation Spectroscopy (HRCCS). Here, the removal of starlight and telluric features is achieved by HRCCS, which correlates the observed sequence of spectra with theoretical templates of exoplanet atmospheres. This takes advantage of different Doppler shifts of the different spectral components. HRCCS helps to disentangle the exoplanet's spectrum from the overwhelming glare of its host star, enabling the study of its physical, chemical, and biological processes. The presence of specific molecules in exoplanet atmospheres may indicate potential biological processes occurring on the planet's surface⁶³. This technique can detect both transiting and non-transiting planets and provides valuable information about the planet's composition, structure, clouds, and dynamics. Recent studies targeted giant planets, led to the detection of various molecules including CO^{55,56,64-68}, H_2O ^{51,65,66,69-73}, CH_4 ⁷¹, HCN^{66,72}, TiO^{53,74}. It is also employed to identify biomarkers and map features in the atmospheres of exoplanets². Six simultaneous species⁵⁷ abundances, including NH_3 , C_2H_2 , and OH detection was previously reported but recently conflicted with JWST observation⁷⁵ where the previous study⁵⁷ did not include a retrieval to formally constrain molecular abundances due to the challenges associated with analyzing high-resolution spectroscopy (HRS) data.

Clouds and haze can disrupt the spectral characteristics, resulting in a flat transmission spectrum^{76,77}. Clouds, formed from particle condensation, exhibit much higher opacity in both absorption and scattering, compared to atmospheric gases. This diminishes the visibility of spectral characteristics, restricting telescopes' access to only the atmospheric layers above clouds⁷⁸. Hazes are particles produced by photochemical reactions that affect opacity across the entire wavelength range. They also cause Rayleigh scattering in the optical spectrum. The featureless spectrum, despite being obtained with sufficient SNR, can be caused by clouds and hazes, which may hinder the diagnosis of the molecular composition of exoplanet atmospheres. Several cooler and smaller exoplanets have shown spectra interpreted as caused by cloudy atmospheres, which poses challenges to constrain chemical species⁷⁹. HRS is a technique to mitigate the effects of clouds and hazes. It leverages its sensitivity to spectral line cores to probe regions situated at higher altitudes above the clouds^{80,81}.

For smaller planets such as mini-Neptunes and super-Earths, so far only upper limits of certainty species in atmospheres⁸² could be established^{83,84}. The measurement is challenging because a small planet's atmosphere absorbs only less than a 1% fraction of the star's light. When observing exoplanets, ground-based telescopes face several challenges: seasonal observability constraints, variations in weather conditions, and the day-to-night cycle⁴⁶. However, despite these limitations, ground-based telescopes have the advantage of being able to detect certain molecules, such as O₂, in the atmospheres of terrestrial exoplanets with the upcoming ELTs instruments suite. This is due to the current generation of space-based spectroscopic instruments such as JWST lacking sensitivity in the O₂ bands.

The scientific case for studying O₂ in the universe has been proposed for a long time. So far it has been found in molecular cloud^{85,86}, nebula⁸⁷ and quasi-stellar object⁸⁸ where the line can be disentangled from a telluric line due to its redshift, enables observation with ground-based millimeter facilities. In exoplanet atmospheres, ozone (O₃) was suggested to be a proxy of oxygen (O₂)^{63,89–91}. However, the recent theoretical work⁹² emphasizes that it is extremely difficult to infer O₂ levels from an O₃ because the condition depends strongly on the stellar type and the incident UV flux. Utilizing a spectrograph with a resolution of R=100,000 on an Extremely Large Telescope (ELT), the endeavor to detect O₂ in exoplanetary atmospheres within a 20-parsec radius will take approximately 60 to 100 years, after relative velocities, planet occurrence rates, and the feasibility of target observations are taken into account⁹³. In an optimistic scenario, with the possibility of combining signals from multiple ELTs, the investigation for TRAPPIST-1d could potentially be accomplished in approximately 16 to 25 years with traditional high-resolution spectrograph on three ELTs. It is previously suggested that the resolution R=300,000-500,000 instrument⁴⁷ will be needed for the next generation ELTs to expedite the observation process. Furthermore, a concept for the next NASA flagship mission⁹⁴ recommended by the National Academies' Pathways to Discovery in Astronomy and Astrophysics for the 2020s, Habitable Worlds Observatory (HWO), also plans to study O₂ in terrestrial exoplanets launch in the 2040s.

To summarize, both transit spectroscopy and reflected light direct imaging techniques strongly benefit from efficient high-resolution spectrographs. This is particularly important if clouds and hazes are as abundant in atmospheres as hinted by recent results, as it also helps boost the signal within the resolved spectral lines. This work delves into the present-day high-resolution instruments employed in the study of exoplanets' atmospheres and outlines a potential solution to overcome the resolution limit for the development of future instruments designed for Earth-analog observation with High-Resolution Spectroscopy (HRS). The techniques for establishing HRS are detailed in Section 2. Section 3 presents the outcomes of the prototype for the future interferometer-based instrument, with the discussion in Section 4.

2 Methods

In this section, we collate state-of-the-art methods to technically achieve HRS. These are then empirically compared in the next section. HRS helps resolve molecular features into individual lines, allowing for a more detailed analysis of the exoplanet's atmosphere. To achieve the utmost precision when utilizing the Doppler Spectrograph for observing slow-rotating, solar-type stars, it is recommended to utilize a spectral resolution of no less than $R = \lambda / \Delta\lambda = 100,000$ ^{1,95}. This level of resolution and sampling frequency not only amplifies the signal-to-noise ratio for each spectral line but also mitigates potential instrumental errors. In making this selection, factors such as telescope mirror size, simultaneous spectral coverage, resolving power, and overall throughput must all be considered carefully. These high-resolution spectrographs can be broadly categorized into two main groups: those reliant on diffraction grating (such as Echelle and Immersion Grating spectrographs) and those based on interferometry, employing either Michelson Interferometers or Fabry-Perot Interferometers.

Most of the recent HRS exoplanet atmosphere observations adopt instruments originally designed for precision radial velocity (PRV). These are optimized to conduct time series observation with long-term stability. Traditionally, the Echelle spectrograph is a preferable option for PRV high-resolution instruments. Echelle spectrographs have hit a limit of resolutions of approximately R=100,000 for telescopes with apertures spanning 6.5 – 10 meters. Some exceptional cases involve the use of a pupil slicer scheme e.g. PEPSI^{109,110,114} or single-mode fiber feeding^{108,111,115}, which has the potential to enhance the resolution to as high as R=250,000. This constraint is predominantly rooted in the principle of etendue preservation ($E = A \times \Omega$ where A is the beam cross-section area and Ω is the solid angle). The challenge becomes pronounced as larger telescope apertures, such as VLTs and ELTs, require the management of more extensive collimated beams, dispersion gratings, and,

Instrument	Telescope & size	Range (μm)	Spectral Resolution
NIRSPEC ⁹⁶	KECK II 10 m	0.95 - 5.50	35,000 ²⁸
UVES ⁹⁷	VLT 8 m	0.30 - 1.10	30,000 - 110,000
HDS ⁹⁸	Subaru 8 m	0.95 - 5.50	160,000
IRD ⁹⁹	Subaru 8 m	0.95 - 1.75	70,000
SPIRou ¹⁰⁰	CFHT 3.58 m	0.98 - 2.35	70,000
CRIRES ¹⁰¹	VLT 8 m	0.95 - 5.20	100,000
CRIRES+ ¹⁰²	VLT 8 m	0.92 - 5.20	100,000
GIANO ¹⁰³	TNG 10 m	0.95 - 2.50	25,000
CARMENES ¹⁰⁴	CAHA 3.5 m	0.52 - 1.71	80,000-100,000
IGRINS ¹⁰⁵	Gemini South 8.1 m	1.45 - 2.45	40,000
HARPS ¹⁰⁶	KECK II 10 m	0.38 - 0.69	115,000
HARPS-N ¹⁰⁷	TNG 10 m	0.38 - 0.69	115,000
PARVI ¹⁰⁸	Hale 5.1 m	1.145 - 1.766	50,000-70,000
EXPRES ¹⁰⁹	Lowell Discovery 4.3 m	0.38 - 0.78	137,000
NIRPS ¹¹⁰	ESO 3.6 m	0.95 - 1.8	100,000
iLocator ^{111, 112}	LBT 2 \times 8 m	0.97 - 1.31	190,000
ESPRESSO ¹¹³	VLT 4 \times 8 m	0.38 - 0.78	70,000 - 200,000
PEPSI ¹¹⁴	LBT 2 \times 8 m	0.38 - 0.91	120,000 - 250,000

Table 1. Ground-based high resolution spectrographs can be used for the exoplanet atmospheres observations.

consequently, a bulkier and heavier spectrograph as a whole. As a result, labor, fabrication, and construction costs increase. This challenge is exacerbated when considering the next-generation Extremely Large Telescope (ELT) because the resolution is inversely related to telescope diameter, as expressed in the relationship $R \propto \frac{1}{D}$ ¹¹⁶ the case of a diffraction-limited instrument. However, currently, all the exoplanet atmosphere observations are based on Echelle or Immersion grating spectrograph as shown in Table 1 with the exception of single-model fiber-fed instruments such as iLocator¹¹¹ and PARVI¹⁰⁸.

For precision and stability, single-mode fibers (SMFs) are considered optimal for guiding light into spectrographs^{117, 118}. The SMF spectrographs operate in the diffraction-limited regime, achieving exceptionally high spectral resolution in a compact instrument. It allows the study and mitigation of stellar variability¹¹¹. However, efficiently coupling a point spread function (PSF) into an SMF poses inherent challenges due to their intrinsic properties¹¹⁹. The theoretical maximum coupling efficiency of an unobstructed circular aperture into an SMF is approximately 81%¹²⁰. In practice, most ground-based telescopes feature obstructed circular apertures and spiders in the pupil, which significantly impact coupling efficiency, for example, resulting in about 60% efficiency at telescopes like Keck and Subaru¹²¹ and approximately 73% at VLT¹²². HiRISE needs a coupling efficiency exceeding 95%¹²² to maximize feasibility to spectrally characterize exoplanets. Achieving this objective requires precise centering of the PSF with the core of the fiber within $0.1 \lambda/D$ ¹¹⁹, which is extremely challenging. A coupling efficiency as low as 59% of the maximum is acceptable for HiRISE, corresponding to a misalignment of $0.2 \lambda/D$ between the PSF and the fiber. In this case, characterizing the most challenging targets would be unfeasible without the required additional telescope time. KPIC reported achieving the placement of the planet's PSF on the science fiber with a precision of less than $0.2 \lambda/D$ ($< 10 \text{ mas}$)²⁸ in the K band.

Fourier Transform Spectrometers (FTS) are based on the principle of the Michelson interferometer. They derive spectral information via an interference-based process and mathematical algorithms. An illumination source is split into two beams via a beam splitter, creating a path difference. The beams recombine, forming an interferogram on a detector. Fourier Transformation converts this time-domain interferogram into a spectrum, revealing spectral properties¹²³. FTS instruments are complex, sensitive to vibrations, and substantial in size¹²⁴. Achieving higher resolution often necessitates elongated optical paths, which can, in turn, impose limitations on the range of accessible wavelengths. The spectral resolution of FTS is determined from the Optical Path Difference (OPD). Primarily owing to their subpar system efficiency of broadband spectroscopy, the use of traditional FTS in stellar astronomy has been limited¹²⁵. The overall on-sky efficiency of the dispersed Fourier transform spectrograph (dFTS), at a spectral resolution of $R = 50,000$, reaches a level of efficiency (4-10%)¹²⁵ similar to that of Echelle spectrographs. Conversely, FTS is highly effective for solar observations, achieving ultra-high spectral resolutions of $R = 700,000$ to $1,000,000$, such as FTS instruments at Kitt Peak¹²⁶ and an FTS from Institut für Astrophysik, Göttingen (IAG)¹²⁷.

The Virtually Imaged Phased Array (VIPA)¹²⁸ functions as an angular dispersive device similar to a prism and diffraction grating. It separates light into its spectral components and operates almost independently of polarization. Unlike prisms or conventional diffraction gratings, the VIPA exhibits significantly higher angular dispersion while possessing a smaller

free spectral range. It also offers structural simplicity and compact dimensions within a reasonable cost range. VIPA is well-suited to serve as the primary dispersion element in ultra-high resolution spectrometers for both ground¹²⁹ and space instruments¹³⁰. Increased spectral resolution may result in decreased wavelength coverage. VIPA spectrographs are well-suited for ultra-high resolution applications but are constrained to a limited spectral range of approximately 200 nm. This spectral limitation may pose challenges when simultaneous observation across a broad wavelength range is required. VIPAs, akin to Fabry-Perot Interferometers (FPI), exhibit sensitivity to input light's spectral characteristics, introducing potential complexities in system alignment. Furthermore, VIPAs can generate intricate fringe patterns in their spectra, demanding specialized analysis methods. Nevertheless, the compact size of VIPA allows for versatile implementation. VIPA technology offers versatility in its application, accommodating both single-mode and multi-mode fiber systems¹³¹, with a potential throughput of up to 40%¹³². Currently, VIPA spectrographs^{131,132} employ diffraction gratings as cross-dispersers. Further improvements in throughput can be achieved by using VPH cross-dispersion.

Current generation ground-based and space-based instrumentation are not yet capable of studying O₂ around Earth-analogs. Alternative approaches and novel instrumentation concepts have been introduced to study O₂ around Earth-analogs with ELT. Firstly, the Fabry Perot Instrument for Oxygen Searches (FIOS)^{48,133} is an FPI based resolution booster designed as a plug-in for the traditional (external) high-resolution spectrograph being built for ELTs to study molecular oxygen with transmission spectroscopy and cross-correlation technique. It splits the signal into multiple, each with a different (shifted) periodic high-resolution profile imposed. Analyzing the spectra of these signals with an external spectrograph gives a higher resolution. It also improves the spectral sampling frequency of the spectral profiles with the chained FPI. In the prototype, the demonstration of FIOS subunit was plugged into a VIPA-based external spectrograph. This resulted in a very compact instrument. This solution could reduce the observation time on the ELT to at least half⁹³ from the signal gain into the high-resolution feature. Secondly, a new collaboration established in 2023 proposed studying O₂ in the atmosphere of the nearest rocky exoplanet, Proxima b, and its analogs using Ultra-fast AO Technology Determination for Exoplanet Imagers from the Ground (UNDERGROUND)¹³⁴. This serves as a test bed for high-contrast imaging and direct spectroscopy. The instrument is designed to achieve a contrast goal of 3×10^{-5} at $10 \lambda/D$, with a combination of ground-based extreme adaptive optics and high-resolution VIPA spectrograph¹³².

In this work, an exposure time calculator (ETC) was developed to numerically assess the benefits of high-resolution spectroscopy for detecting molecular oxygen in exoplanet atmospheres, comparing oxygen-rich and oxygen-free models at the O₂ A-band. The calculation method follows the IGRINS' ETC¹³⁵, which has already been applied to other instruments^{136,137}, with adjustments for high-resolution features by summing the signal from all spectral lines within the oxygen A-band. The O₂ ETC is optimized for simulating the signal-to-noise sensitivity per resolution element at the Oxygen A-band, comparing an oxygen atmosphere model with a no-oxygen atmosphere. In addition to the cross-correlation technique, the likelihood method performs comparably well for template comparisons⁷⁷. In this simulation, the process involves comparing two models: one containing O₂ absorption features and another without. The code calculates the difference in chi-squared values ($\Delta\chi^2$) between these model spectra calculated with ESO SkyCalc¹³⁸⁻¹⁴⁰.

$$\Delta\chi^2 = \Sigma\left(\frac{data - signal_{NoO_2}}{Noise}\right)^2 - \Sigma\left(\frac{data - signal_{O_2}}{Noise}\right)^2 \quad (2)$$

A Monte Carlo method is used to generate simulated data by sampling from a normal distribution centered on the signal with O₂ and the given noise level. The $\Delta\chi^2$ is computed for each simulated dataset showing the difference between the chi-squared values for the no-O₂ model and the O₂ model as shown in Equation 2 and averaged over 1000 data realizations.

This simplified calculation does not account for telluric contamination in ground-based observations, making it applicable for both space- and ground-based observations. Telluric effects were addressed in a previous study⁴⁶. Here the calculation is focused on half of the Oxygen band (0.766 - 0.772 μm), where the O₂ absorption with the airmass=1 model of ESO SkyCalc is not saturated to complete absorption. Nevertheless, our exposure estimates should generalize approximately proportionally to the full oxygen band. The calculation incorporates realistic parameters for modern spectrograph components, such as low read-noise (1 electrons) CMOS detectors and reduced dark current (0.1 electrons/sec) levels due to detector cooling. The calculation assumes an 8-meter telescope with different instrument resolutions assuming 1% transit depth with thermal noise excluded, as the effect start from H band (1.4 μm) onward¹³⁸.

The comparison using the exposure time calculator focuses solely on the instrument's signal for oxygen observation. In practice, spectral information from exoplanet atmospheres is further degraded by telluric lines (from Earth). Simulations have already been conducted to account for these effects, such as different levels of cloud impacts⁴⁶ and haze, which can suppress up to 50% of spectral features⁷⁷ in the case of $3 \times$ planet's isolation. The previous work⁷⁷ presented several haze scenarios motivated by observations of featureless spectra. Atmospheric transmissivity (shown in Figure 3 for Earth) is affected such that the upper half is cut off and set to a constant (see Figure 4 in the previous work⁷⁷). Similarly, the simulation here considers three scenarios: a clear atmosphere without haze or clouds (optimistic case), 50% haze (realistic case), and 90% haze (pessimistic case). The percentage indicates how the O₂ transmissivity is clipped. Figure 3 left panel illustrates the assumed transit depth for the three scenarios (blue, purple, and red curves).

3 Results

In this work, we compare and contrast current and upcoming dispersing techniques for high-resolution spectroscopy. This section reviews Echelle-based and interferometry-based instruments, such as Fourier Transform Spectrograph (FTS) and Fabry-Perot Interferometer (FPI). In the results section, we compare their effectiveness in achieving exceptionally high-resolution spectral profiles empirically. For this purpose, we compare telluric oxygen observations taken by an Echelle spectrograph, X-shooter, to assess the level of low-medium resolution against the ultra-high resolution from FIOS-demo and FTS spectrograph. We note here that typical Echelle spectrographs nowadays can reach $R=100,000$, as shown in Table 1. In some exceptional cases, it is limited to $R=200,000$.

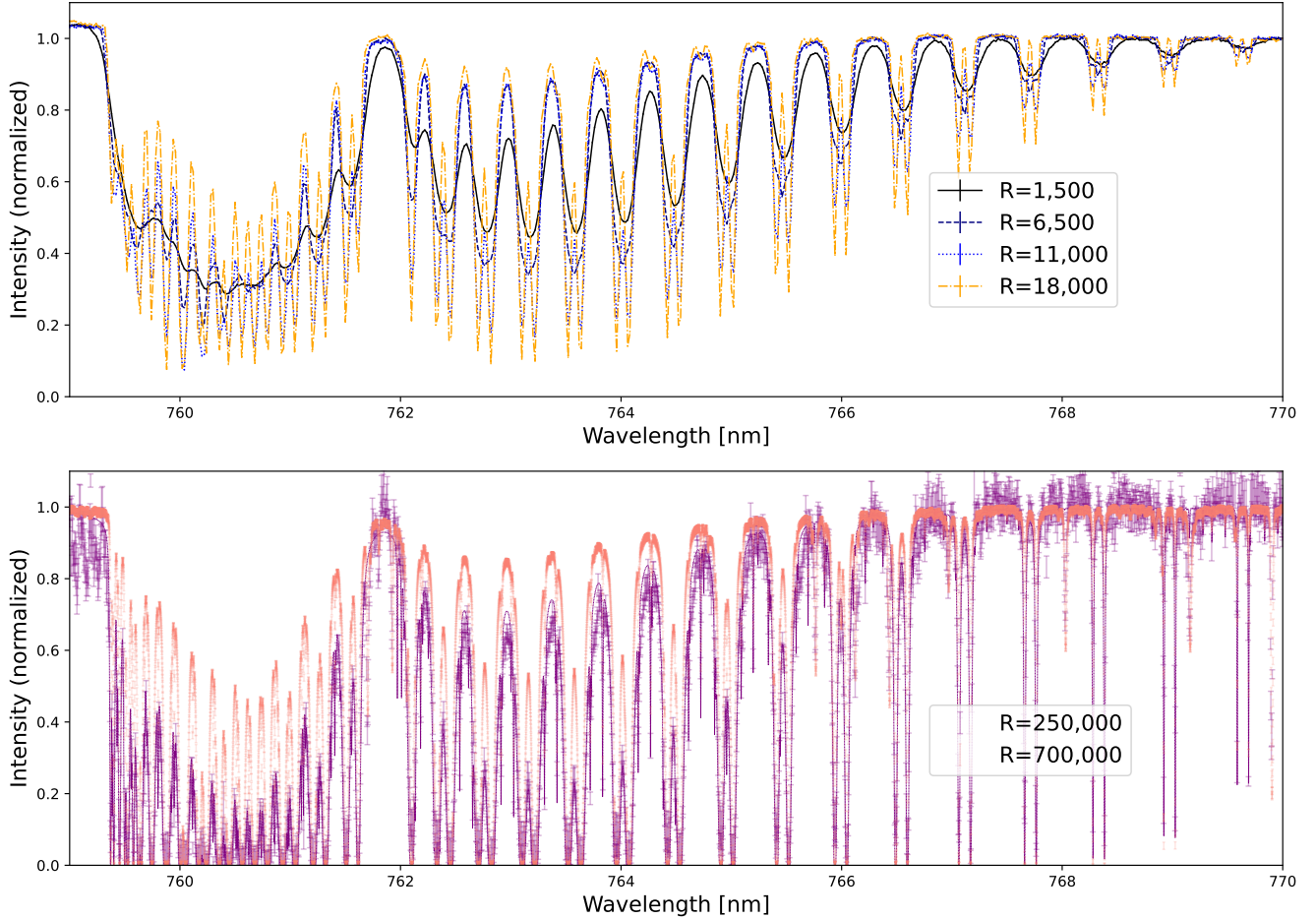


Figure 2. Comparison of (telluric) molecular oxygen spectrum observed using low-medium resolution spectrograph and interferometer-based instruments. The top panel shows the observed telluric spectrum from archival X-Shooter spectra with spectral resolution ranging from $R=1500$ to $R=18000$ in different colors. The lower panel shows the spectrum from FTS¹²⁶ (red) with $R=700,000$ and FIOS-demo¹³³ (purple) with $R=250,000$ overlaid with a fitted model. Note that the two observations were taken at different altitudes, which explains the differences in the line depths of the features.

Figure 2 illustrates a comparison between the observed low-medium resolution and the high-resolution spectral profiles of the oxygen A band, depicting observations of (telluric) molecular oxygen. The upper panel of Figure 2 shows low to medium resolution telluric oxygen features. These were obtained from the ESO Science Archive Facility using X-shooter¹⁴¹ observations during February and March 2024 by the UVES team, as part of Program ID: 60.A-9022(c), OB ID:2024672, 2024624 and 2024822, at various resolutions with short exposures (12 seconds). The results indicate that higher resolution enables the observation of more detailed features within the molecular oxygen spectrum, revealing the signal more distinctly within each spectral line. The lower panel of Figure 2 shows performance tests for future HRS instrumentation by observing the Sun through the Earth's atmosphere. These profiles demonstrate the measurement outcomes obtained using two types of interferometers: Michelson-based and FPI-based. Firstly, the FTS from the National Solar Observatory at Kitt Peak¹²⁶ reported $R=700,000$ in the oxygen A-band. Secondly, the FIOS-demo¹³³ showcases spectral profiles based on a chained FPI array with a

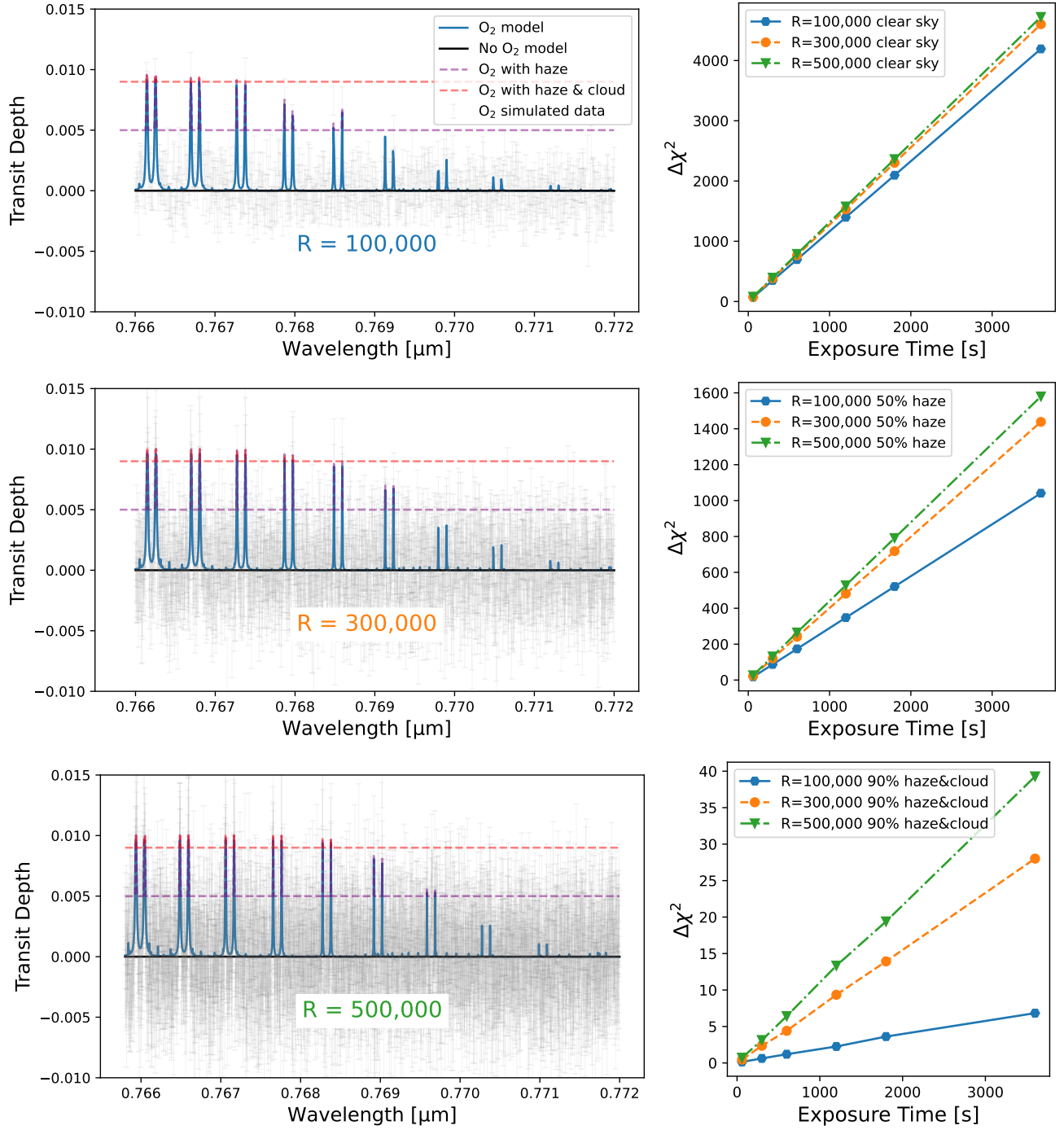


Figure 3. Comparison of transit depth observed at different spectral resolutions: $R=100,000$ (top left panel, blue line in the right panels), $R=300,000$ (middle left panel, orange line in the right panels), and $R=500,000$ (bottom left panel, green line in the right panels), assuming 1% of the star's light passes through the exoplanet's atmosphere. Left panels: simulated model comparison of transit spectral features for different scenarios—No- O_2 (black solid line), clear sky O_2 (blue solid line), simulated data for the corresponding resolution (grey data points), signal clipped by 50% due to haze (purple dashed line), and signal clipped by 90% due to haze and cloud deck combined (red dashed line). Right panels: model comparison confidence with the different resolutions as the exposure time increases. The three observing conditions, with clear sky (top right panel), 50% haze (middle right panel) and haze&cloud (bottom right panel)

spectral resolution of $R=250,000$. This resolution can potentially increase up to $R=350,000$ with the addition of each array. The throughput of each additional unit, however, decreases by 10-15%⁵⁰. One benefit of achieving this level of resolution is the increase in signal-to-noise ratio and the sampling frequency for each spectral line, which may reduce the required observing time, as predicted in^{46,93}.

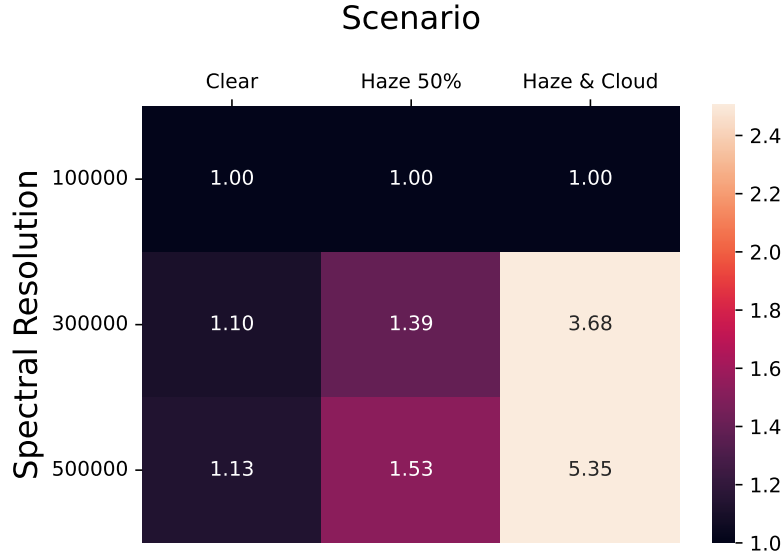


Figure 4. Exposure time reduction factors. Columns indicate the considered scenarios: clear atmosphere (optimistic case), 50% haze (realistic case), and 90% haze (pessimistic case) at different instrument spectral resolutions ($R=100,000$, $R=300,000$, $R=500,000$) with a 10-minute exposure. The ratio represents the performance of ultra-high resolutions compared to $R=100,000$.

The results from the exposure time calculator are presented in Figure 3. The left panels display the non-saturated region of the oxygen A-band signal at different resolutions: $R=100,000$, $R=300,000$, and $R=500,000$. These are compared with scenarios where haze reduces the signal by 50% (50% haze), and haze combined with a cloud deck suppresses 90% (90% haze and cloud) or more of the signal. The figure demonstrates that higher resolution provides more data points, thereby increasing the sampling frequency, as indicated by the increasing number of grey data points with higher resolution. For the model template matching, the right panels show the likelihood results ($\Delta\chi^2$) for different cloud and haze scenarios on the planet. For clear skies, increasing the resolution from $R=100,000$ to $R=300,000$ enhances $\Delta\chi^2$ by approximately 9-10%, with a further increase to $R=500,000$ improving it by 11-12%. Conversely, the exposure time can be reduced with higher resolution by these factors, because the relation between exposure time and $\Delta\chi^2$ significance level is linear.

The impact of resolution becomes more pronounced under hazy and cloudy conditions. In the realistic 50% haze scenario where only half of the O₂ signal is observable, increasing the resolution from $R=100,000$ to $R=300,000$ reduces the necessary exposure time by about 34%, and to 50% at $R=500,000$. In the most challenging scenario, where less than 10% of the signal is observable due to haze and cloud cover, resolution increases from $R=100,000$ to $R=300,000$ can enhance 3.7 times of the signal and about 5 times at $R=500,000$. This is also summarized in Figure 4 as a ratio selected for the case of 10 minute exposures. Other exposures give similar results since the linear relationship results in similar outcomes for each exposure time interval. The current calculated range focuses only on the non-saturated portion (half of the oxygen band) due to limitations in the simulated data, where the saturated part cannot be accurately compared across different resolutions. If the entire band could be observed without saturation, these ratios are expected to improve further.

4 Discussion

4.1 Performance of current generation instruments

Ground-based and space-based observations offer complementary insights. By combining low- and high-resolution observations, we can attain more precise and accurate insights spanning from the lower to the upper atmosphere¹⁵⁴. High-resolution ground-based observations provide a distinctive window into the thermospheres of exoplanets and exhibit sensitivity to alkali element abundances. This could be meticulously analyzed in conjunction with lower-resolution observations¹⁵⁵. While space-based instruments mitigate the telluric interference issue, their current instrumental constraints (typically $R=100$ up to $R\sim 3,000$) restrict their ability to capture detailed spectral features. The Wide Field Camera 3 (WFC3)¹⁵⁶ on the Hubble Space Telescope

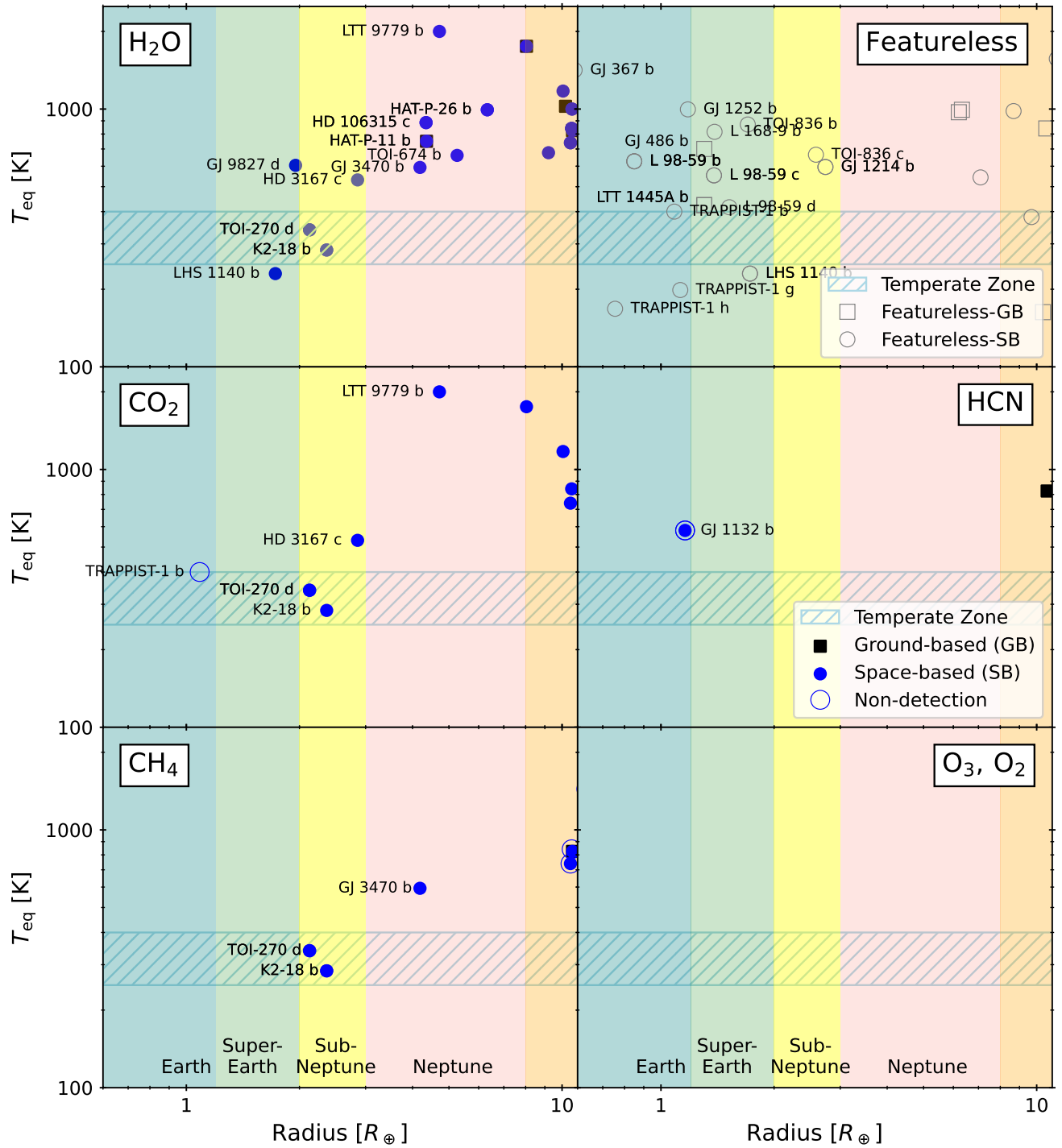


Figure 5. Detection of molecules prominently involved in biological processes on Earth using current instrumentation: H₂O^{142–150}, CH₄¹⁵¹, CO₂^{144,150,152}, HCN¹⁵³, O₂, O₃ and featureless of Earth- to Neptune-size planets using ground-based (black square) and space-based (blue circle) instruments. Data retrieved from ExoAtmospheres Database as of September 2024

(HST) remains one of the most successful instruments for studying exoplanet atmospheres, including alkali element analysis⁴⁴, particularly in the Neptune and sub-Neptune regime. Meanwhile, JWST is poised to advance the characterization of Earth and Super-Earth regimes.

Upcoming space-based instrumentation is dedicated to exoplanetary atmospheres using low-resolution spectrographs. These include the Colorado Ultraviolet Transit Experiment (CUTE)¹⁵⁷, the Atmospheric Remote-Sensing Infrared Exoplanet Large-survey mission (ARIEL)¹⁵⁸ and Twinkle¹⁵⁹. The CUTE CubeSat project concentrates on the near-ultraviolet region (0.25 to 0.33 μm) with a spectral resolution of 3,000. In the near future, the ARIEL mission, scheduled for a 2029 launch, focuses on a broader wavelength range spanning from 0.5 to 7.8 μm , albeit with a maximum resolution of $R = 100$. This mission has the ambitious goal of studying 1,000 large planets, including a select few Earth-sized ones¹⁵⁸. The Twinkle mission will be equipped with a 0.45 m telescope and a spectrometer, providing simultaneous wavelength coverage from 0.5 to 4.5 μm . Currently, the transit photometry monitoring space mission, TESS¹⁶⁰ and CHEOPS¹⁶¹ offer a wealth of suitable targets for forthcoming instruments tailored to the spectral characterization of exoplanetary atmospheres.

The time is ripe for considering the initiation of a specialized effort aimed at the thorough characterization of prominent molecules which are measurable indicators of biological processes, conditions, or so-called biomarkers. A theoretical study⁶³ proposed that the concurrent identification of O_2 , O_3 , H_2O , CO_2 and CH_4 in the absence of CO might signify conditions reminiscent of those found on Earth. Remarkably, the first detection of these biomarkers around small planets using space-based instrumentation have been reported. Figure 5 illustrates the current study of biomarkers by reported detection as listed in the ExoAtmospheres Database. Detections are more abundant in gas giants and at high surface temperatures, corresponding to larger stellar transit absorption signals. The dearth of detections in super-Earths and sub-Neptunes highlights the ongoing challenges. Focusing on the detection of molecules to-date in small-sized planets, H_2O has been detected in several Neptune-sized planets: HAT-P-26b^{142, 162}, HD106315c¹⁴⁵, HAT-P-11b^{142, 163}, TOI-674b¹⁴⁹. The 3σ detection of H_2O on LTT9779b¹⁴⁴ with Hubble Space Telescope's HST/WFC3, appears featureless¹⁶⁴ with JWST Near-Infrared Imager and Slitless Spectrograph (NIRISS). It is also detected in sub-Neptune planets TOI-270d^{146, 165, 166}, K2-18b^{143, 167}. A recent study on K2-18b¹⁵² suggests it is a Hycean planet. For super-Earth, H_2O is detected in GJ9827d¹⁴⁷ and LHS1140b¹⁴⁸ with HST while using JWST¹⁶⁸ shows no absorption feature although data favor an N_2 -dominated atmosphere with H_2O and CO_2 . The search for CO_2 has been found in K2-18b¹⁵², TOI-270d^{165, 166} and LTT9779b with 2.4σ detection from HST/WFC3 G102 ($R=210$ at 1000 nm) and G141 ($R=130$ at 1400) grisms μm but appear featureless¹⁶⁴ due to cloud from one transit observation with JWST NIRISS ($R=700$) slitless spectroscopy mode. The observations on the Earth-size planet TRAPPIST-1b found little to no atmosphere and no CO_2 ¹⁶⁹ was detected with JWST-Mid-Infrared Instrument (MIRI) and featureless¹⁷⁰ spectra with JWST NIRISS. CH_4 ^{165, 166} were detected in TOI-270d with JWST-Near-Infrared Spectrograph (NIRSPEC) ($R=1000-2700$) and K2-18b^{152, 171} with both HST and JWST NIRISS. For HCN detection on 55 Cancri e¹⁵³ with HST but not yet seen from ground-based observation¹⁷². The detection on GJ1132b has been under debate^{151, 173, 174}. A few studies have reported the detection of CO in Neptune size planets e.g. detection in GJ3470b¹⁷⁵ and upper limit in GJ436b¹⁷⁶. However, this is not entirely unexpected; for instance, in Earth-like scenario, the presence of CO in the atmosphere is generally undesirable⁶³. The featureless corner reported attempts to measure rocky planets with featureless spectra^{170, 177-185}. This could be interpreted as: 1) it's cloudy and hazy, 2) there are no atmospheres around these rocky bodies due to the host star, and 3) we have reached the instrument's limit, since the rocky atmospheres are supposed to be so small compared to the rocky planet's radius. From Figure 3, we can also observe that the current limitations of ground-based observations rarely extend to measurements below those of Neptune size planets except for the LTT1445Ab¹⁸³ and GJ486b¹⁸⁵ with featureless spectra. This study demonstrates that high spectral resolution is particularly advantageous in hazy and cloudy scenarios. Future instruments should prioritize a combination of large aperture, high throughput, and high resolution to further enhance observational capabilities.

4.2 Future development for O_2 detection

Motivated by the apparent ubiquity of haze and clouds, we demonstrate the need for $R = 100,000$ spectroscopy with detailed exposure time simulations. In our optimistic, realistic and pessimistic scenarios, $R > 300,000$ spectrographs give a exposure time reduction of 1.1, 2x and 4x compared to $R = 100,000$ spectrographs for the detection of O_2 .

With detailed and realistic exposure time calculations, we confirm and extend previous findings^{46, 77, 93, 186} that HRS improves biosignature detection also in the Oxygen A-band. One early study¹⁸⁶ examined different oxygen bands at varying resolutions using model spectra for different stellar types suggesting that ultra-high resolution could reduce over 30% in the number of transits required to produce a detection. A subsequent study⁷⁷ simulated realistic Earth-like planet spectra, focusing on molecules other than oxygen, with resolutions up to $R = 100,000$ using existing telescopes with possible hazy scenarios. Similarly, the third study⁴⁶ modeled the ELTs' performance for transit spectroscopy at $R = 100,000$, suggesting that increasing the resolution to $R = 300,000$ doubles the line depth compared to $R = 100,000$ and can also reduce the required transit time by 30%. However, the spectral lines do not gain much additional information by further increasing the resolution to $R = 500,000$. Finally, the most recent work⁹³ explored a survey of molecular oxygen using ELTs, comparing resolutions of $R = 100,000$ and $R = 500,000$ for clear sky conditions. In hazy and cloudy conditions, as shown in Figure 3, ultra-high resolutions of $R = 300,000-400,000$ demonstrate significant advantages in capturing diluted signals. This calculation is applicable to ground-based high-resolution observations of small planets using both transmission spectroscopy and reflected light, as well as space-based observations to

velocity method, and the characterization of exoplanetary atmospheres¹⁹¹. Multi-channel VIPA spectrographs can be used for the simultaneous observation of multiple biomarkers. An alternative proposal for utilizing interferometry-based instruments in space involves Imaging Fourier Transform Spectrographs (iFTS). These instruments are generally less susceptible to detector noise and offer several other advantages, including simultaneous imaging and spectroscopy, reduced detector size requirements, and adjustable spectral resolution. By comparing analytic and numerical models of Integral Field Spectrographs (IFS) and iFTS, it is determined that iFTS would be more efficient than an IFS if the readout noise of near-IR detectors is halved from the current state-of-the-art level (readout noise above 2-3 electrons/pix/frame)¹⁹². Lastly, for the study of the atmosphere, especially for terrestrial exoplanets in the temperate zone, large mirror apertures are a necessity. The lightweight segmented space telescopes created through additive manufacturing¹⁹³ could emerge as a pivotal contributor.

5 Conclusion

In this work, we provided an overview of current and upcoming technical capabilities for characterizing exoplanet atmospheres around rocky planets. Both direct imaging and transit spectroscopy can greatly benefit from high-resolution, high-throughput spectrographs. We then compared current state-of-the-art on-sky spectra that demonstrate the range of technical capabilities. Our focus was particularly on O₂, which complements already detected atmospheric molecules for a comprehensive characterization of star-planet interaction, geological processes, and potential biological activity. We highlight significant instrumentation advancements and challenges in the field of exoplanet atmosphere studies, particularly focusing on rocky exoplanets. Researchers are continually pushing the boundaries of our understanding of distant worlds through the utilization of grating-based and interferometer-based high-resolution spectroscopy, as well as innovative techniques in high-contrast imaging. The detection and characterization of molecules such as water H₂O, methane CH₄, and oxygen O₂ provide crucial insights into the composition to infer potential habitability of exoplanet atmospheres. However, challenges such as clouds, haze resulting in featureless spectra, and instrumental limitations persist, underscoring the need for further technological innovation and observational refinement. Despite these challenges, advancements in technology and instrument development, particularly with the advent of novel instrument suites on Extremely Large Telescopes (ELTs) and next-generation space-based instruments such as Habitable Worlds Observatory (HWO), offer promising prospects for overcoming these obstacles.

With detailed exposure time calculations for detecting O₂, at the same exposure time, a spectral resolution of 300,000 achieves higher significance compared to 100,000. For the optimistic case of clear skies, the exposure time is reduced by 10%, while in the realistic 50% haze scenario, the required exposure time decreases by 30%. In the most challenging haze and cloud scenario, increasing the resolution from R=100,000 to R=300,000 enables significant detection with 4 times shorter exposure time (and thus correspondingly fewer transits). Therefore, HWO should consider incorporating a high-resolution instrument, as recommended in the 2018 Exoplanet Science Strategy report⁹⁵. Although telluric contamination is not a concern in space, a high-resolution compact instrument would be advantageous for biomarker observations.

As we continue to unravel the mysteries of exoplanetary atmospheres, each discovery brings us closer to unlocking the secrets of other worlds and exploring the potential for life beyond our solar system. Collaboration among astronomers and engineers remains crucial for making significant strides in this field.

References

1. Pepe, F., Ehrenreich, D. & Meyer, M. R. Instrumentation for the detection and characterization of exoplanets. *Nature* **513**, 358–366, DOI: [10.1038/nature13784](https://doi.org/10.1038/nature13784) (2014). [1409.5266](https://doi.org/10.1038/nature13784).
2. Birkby, J. L. Exoplanet Atmospheres at High Spectral Resolution. *arXiv e-prints* arXiv:1806.04617, DOI: [10.48550/arXiv.1806.04617](https://doi.org/10.48550/arXiv.1806.04617) (2018). [1806.04617](https://doi.org/10.48550/arXiv.1806.04617).
3. Follette, K. B. An introduction to high contrast differential imaging of exoplanets and disks. *Publ. Astron. Soc. Pac.* **135**, 093001, DOI: [10.1088/1538-3873/aceb31](https://doi.org/10.1088/1538-3873/aceb31) (2023).
4. Fischer, D. A. *et al.* Exoplanet Detection Techniques. In Beuther, H., Klessen, R. S., Dullemond, C. P. & Henning, T. (eds.) *Protostars and Planets VI*, 715–737, DOI: [10.2458/azu_uapress_9780816531240-ch031](https://doi.org/10.2458/azu_uapress_9780816531240-ch031) (2014). [1505.06869](https://doi.org/10.2458/azu_uapress_9780816531240-ch031).
5. Macintosh, B. *et al.* Discovery and spectroscopy of the young jovian planet 51 eri b with the gemini planet imager. *Science* **350**, 64–67, DOI: [10.1126/science.aac5891](https://doi.org/10.1126/science.aac5891) (2015).
6. Franson, K. *et al.* Astrometric accelerations as dynamical beacons: A giant planet imaged inside the debris disk of the young star af lep. *The Astrophys. J. Lett.* **950**, L19, DOI: [10.3847/2041-8213/acd6f6](https://doi.org/10.3847/2041-8213/acd6f6) (2023).
7. Guyon, O. Extreme Adaptive Optics. *ARAA* **56**, 315–355, DOI: [10.1146/annurev-astro-081817-052000](https://doi.org/10.1146/annurev-astro-081817-052000) (2018).
8. Fusco, T. *et al.* High-order adaptive optics requirements for direct detection of extrasolar planets: Application to the SPHERE instrument. *Opt. Express* **14**, 7515, DOI: [10.1364/OE.14.007515](https://doi.org/10.1364/OE.14.007515) (2006).
9. Graham, J. R. *et al.* Ground-based direct detection of exoplanets with the gemini planet imager (gpi) (2007). [0704.1454](https://doi.org/10.1038/nature04004).

10. Macintosh, B. *et al.* First light of the gemini planet imager. *proceedings Natl. Acad. Sci.* **111**, 12661–12666 (2014).
11. Currie, T. *et al.* Scexao: First results and on-sky performance. *Proc. Int. Astron. Union* **8**, 34–35, DOI: [10.1017/S1743921313007746](https://doi.org/10.1017/S1743921313007746) (2013).
12. Beuzit, J.-L. *et al.* Sphere: the exoplanet imager for the very large telescope. *Astron. & Astrophys.* **631**, A155, DOI: [10.1051/0004-6361/201935251](https://doi.org/10.1051/0004-6361/201935251) (2019).
13. Lyot, B. The Study of the Solar Corona and Prominences without Eclipses (George Darwin Lecture, delivered by M. Bernard Lyot, Assoc.R.A.S., on 1939 May 12). *Mon. Notices Royal Astron. Soc.* **99**, 580–594, DOI: [10.1093/mnras/99.8.580](https://doi.org/10.1093/mnras/99.8.580) (1939). <https://academic.oup.com/mnras/article-pdf/99/8/580/3790591/mnras99-0580.pdf>.
14. Kasdin, N. J., Vanderbei, R. J., Spergel, D. N. & Littman, M. G. Extrasolar planet finding via optimal apodized-pupil and shaped-pupil coronagraphs. *The Astrophys. J.* **582**, 1147, DOI: [10.1086/344751](https://doi.org/10.1086/344751) (2003).
15. Yang, W. & Kostinski, A. B. One-sided achromatic phase apodization for imaging of extrasolar planets. *The Astrophys. J.* **605**, 892 – 901 (2004).
16. Guyon, O. Phase-induced amplitude apodization of telescope pupils for extrasolar terrestrial planet imaging. *Astron. & Astrophys.* **404**, 379–387, DOI: [10.1051/0004-6361:20030457](https://doi.org/10.1051/0004-6361:20030457) (2003).
17. Martinache, F. Pizza: a phase-induced zonal zernike apodization designed for stellar coronagraphy. *J. Opt. A: Pure Appl. Opt.* **6**, 809 – 814 (2004).
18. Ruffio, J.-B. *et al.* Radial velocity measurements of hr 8799 b and c with medium resolution spectroscopy. *The Astron. J.* **158**, 200 (2019).
19. Dekany, R. *et al.* Palm-3000: Exoplanet adaptive optics for the 5 m hale telescope. *The Astrophys. J.* **776**, 130, DOI: [10.1088/0004-637X/776/2/130](https://doi.org/10.1088/0004-637X/776/2/130) (2013).
20. Currie, T. A pathfinder for imaging exo-earths. *Nat. Astron.* **3**, 463–463 (2019).
21. Chauvin, G. *et al.* Discovery of a warm, dusty giant planet around hip 65426. *Astron. & Astrophys.* **605**, L9, DOI: [10.1051/0004-6361/201731152](https://doi.org/10.1051/0004-6361/201731152) (2017).
22. Sparks, W. B. & Ford, H. C. Imaging spectroscopy for extrasolar planet detection. *The Astrophys. J.* **578**, 543–564, DOI: [10.1086/342401](https://doi.org/10.1086/342401) (2002).
23. Riaud, P. & Jean, S. Improving earth-like planets’ detection with an elt: The differential radial velocity experiment. *Astron. & Astrophys. - ASTRON ASTROPHYS* **469**, 355–361, DOI: [10.1051/0004-6361:20077085](https://doi.org/10.1051/0004-6361:20077085) (2007).
24. Snellen, I. *et al.* Combining high-dispersion spectroscopy with high contrast imaging: Probing rocky planets around our nearest neighbors. *Astronomy and Astrophysics* **576**, A59, DOI: [10.1051/0004-6361/201425018](https://doi.org/10.1051/0004-6361/201425018) (2015). [1503.01136](https://arxiv.org/abs/1503.01136).
25. Wang, J., Mawet, D., Ruane, G., Hu, R. & Benneke, B. Observing Exoplanets with High Dispersion Coronagraphy. I. The Scientific Potential of Current and Next-generation Large Ground and Space Telescopes. *AJ* **153**, 183, DOI: [10.3847/1538-3881/aa6474](https://doi.org/10.3847/1538-3881/aa6474) (2017). [1703.00582](https://arxiv.org/abs/1703.00582).
26. Vigan, A. *et al.* First light of vlt/hirise: High-resolution spectroscopy of young giant exoplanets. *A@AND@A* **682**, A16, DOI: [10.1051/0004-6361/202348019](https://doi.org/10.1051/0004-6361/202348019) (2024).
27. Kotani, T. *et al.* Extremely high-contrast, high spectral resolution spectrometer REACH for the Subaru Telescope. In Schreiber, L., Schmidt, D. & Vernet, E. (eds.) *Adaptive Optics Systems VII*, vol. 11448 of *Society of Photo-Optical Instrumentation Engineers (SPIE) Conference Series*, 1144878, DOI: [10.1117/12.2561755](https://doi.org/10.1117/12.2561755) (2020).
28. Delorme, J.-R. *et al.* Keck Planet Imager and Characterizer: a dedicated single-mode fiber injection unit for high-resolution exoplanet spectroscopy. *J. Astron. Telesc. Instruments, Syst.* **7**, 035006, DOI: [10.1117/1.JATIS.7.3.035006](https://doi.org/10.1117/1.JATIS.7.3.035006) (2021). [2107.12556](https://arxiv.org/abs/2107.12556).
29. Finnerty, L. *et al.* Characterizing Hot Jupiter Atmospheres at high resolution with Keck/KPIC. *Bull. AAS* **55** (2023). <https://baas.aas.org/pub/2023n2i324p08>.
30. Lovis, C. *et al.* Atmospheric characterization of proxima b by coupling the sphere high-contrast imager to the espresso spectrograph. *Astron. & Astrophys.* **599**, A16, DOI: [10.1051/0004-6361/201629682](https://doi.org/10.1051/0004-6361/201629682) (2017).
31. Chazelas, B. *et al.* RISTRETTO: seven spaxel single mode spectrograph design. In Evans, C. J., Bryant, J. J. & Motohara, K. (eds.) *Ground-based and Airborne Instrumentation for Astronomy IX*, vol. 12184 of *Society of Photo-Optical Instrumentation Engineers (SPIE) Conference Series*, 121844T, DOI: [10.1117/12.2629907](https://doi.org/10.1117/12.2629907) (2022). [2208.14875](https://arxiv.org/abs/2208.14875).
32. Eisenhauer, F. *et al.* GRAVITY: Observing the Universe in Motion. *The Messenger* **143**, 16–24 (2011).
33. Eisenhauer, F. *et al.* GRAVITY+: Towards Faint Science, All Sky, High Contrast, Milli-Arcsecond Optical Interferometric Imaging. White Paper based on the GRAVITY+ proposal to ESO (2020).
34. Wagner, K. *et al.* Imaging low-mass planets within the habitable zone of α Centauri. *Nat. Commun.* **12**, 922, DOI: [10.1038/s41467-021-21176-6](https://doi.org/10.1038/s41467-021-21176-6) (2021). [2102.05159](https://arxiv.org/abs/2102.05159).

35. Thatte, N. *et al.* Harmoni: the elt's first-light near-infrared and visible integral field spectrograph. *Publ. The Messenger* vol. 182 pp. 7–12, March 2021., DOI: [10.18727/0722-6691/5215](https://doi.org/10.18727/0722-6691/5215) (2021).
36. Bidot, A., Mouillet, D. & Carlotti, A. Exoplanet detection limits using spectral cross-correlation with spectro-imaging. Analytical model applied to the case of ELT/HARMONI. *Astronomy and Astrophysics* **682**, A10, DOI: [10.1051/0004-6361/202346185](https://doi.org/10.1051/0004-6361/202346185) (2024). [2311.13275](https://arxiv.org/abs/2311.13275).
37. Vaughan, S. R. *et al.* Behind the mask: can HARMONI@ELT detect biosignatures in the reflected light of Proxima b? *MNRAS* **528**, 3509–3522, DOI: [10.1093/mnras/stae242](https://doi.org/10.1093/mnras/stae242) (2024). [2401.09589](https://arxiv.org/abs/2401.09589).
38. Brandl, B. *et al.* Metis: The mid-infrared elt imager and spectrograph. *Publ. The Messenger* vol. 182 pp. 22–26, March 2021., DOI: [10.18727/0722-6691/5218](https://doi.org/10.18727/0722-6691/5218) (2021).
39. Marconi, A. *et al.* ANDES, the high resolution spectrograph for the ELT: science case, baseline design and path to construction. In Evans, C. J., Bryant, J. J. & Motohara, K. (eds.) *Ground-based and Airborne Instrumentation for Astronomy IX*, vol. 12184 of *Society of Photo-Optical Instrumentation Engineers (SPIE) Conference Series*, 1218424, DOI: [10.1117/12.2628689](https://doi.org/10.1117/12.2628689) (2022).
40. Palte, E. *et al.* Ground-breaking exoplanet science with the andes spectrograph at the elt (2023). [2311.17075](https://arxiv.org/abs/2311.17075).
41. Stevens, D. J. & Gaudi, B. S. A Posteriori Transit Probabilities. *PASP* **125**, 933, DOI: [10.1086/672572](https://doi.org/10.1086/672572) (2013). [1305.1298](https://arxiv.org/abs/1305.1298).
42. Saxena, P., Villanueva, G. L., Zimmerman, N. T., Mandell, A. M. & Smith, A. J. R. W. Simulating reflected light exoplanet spectra of the promising direct imaging target, andromedae d, with a new, fast sampling method using the planetary spectrum generator. *The Astron. J.* **162**, 30, DOI: [10.3847/1538-3881/abf657](https://doi.org/10.3847/1538-3881/abf657) (2021).
43. Seager, S. & Sasselov, D. D. Theoretical Transmission Spectra during Extrasolar Giant Planet Transits. *ApJ* **537**, 916–921, DOI: [10.1086/309088](https://doi.org/10.1086/309088) (2000). [astro-ph/9912241](https://arxiv.org/abs/astro-ph/9912241).
44. Charbonneau, D., Brown, T. M., Noyes, R. W. & Gilliland, R. L. Detection of an Extrasolar Planet Atmosphere. *ApJ* **568**, 377–384, DOI: [10.1086/338770](https://doi.org/10.1086/338770) (2002). [astro-ph/0111544](https://arxiv.org/abs/astro-ph/0111544).
45. Boldt-Christmas, L. *et al.* Optimising spectroscopic observations of transiting exoplanets. *Astronomy and Astrophysics* **683**, A244, DOI: [10.1051/0004-6361/202347398](https://doi.org/10.1051/0004-6361/202347398) (2024). [2312.08320](https://arxiv.org/abs/2312.08320).
46. Currie, M. H., Meadows, V. S. & Rasmussen, K. C. There's More to Life than O₂: Simulating the Detectability of a Range of Molecules for Ground-based, High-resolution Spectroscopy of Transiting Terrestrial Exoplanets. *PSJ* **4**, 83, DOI: [10.3847/PSJ/acccf86](https://doi.org/10.3847/PSJ/acccf86) (2023). [2304.10683](https://arxiv.org/abs/2304.10683).
47. Lopez-Morales, M. *et al.* Detecting earth-like biosignatures on rocky exoplanets around nearby stars with ground-based extremely large telescopes. *Bull. AAS* **51** (2019). <https://baas.aas.org/pub/2020n3i162>.
48. Ben-Ami, S., López-Morales, M., Garcia-Mejia, J., Abad, G. G. & Szentgyorgyi, A. High-resolution spectroscopy using fabry–perot interferometer arrays: An application to searches for o₂ in exoplanetary atmospheres, DOI: [10.3847/1538-4357/aac835](https://doi.org/10.3847/1538-4357/aac835) (2018).
49. Szentgyorgyi, A. *et al.* The GMT-Consortium Large Earth Finder (G-CLEF): an optical Echelle spectrograph for the Giant Magellan Telescope (GMT). In *Ground-based and Airborne Instrumentation for Astronomy VI*, vol. 9908 of *Proc. SPIE*, 990822, DOI: [10.1117/12.2233506](https://doi.org/10.1117/12.2233506) (2016).
50. Rukdee, S. *et al.* Characterization of a multi-etalon array for ultra-high resolution spectroscopy. In Evans, C. J., Bryant, J. J. & Motohara, K. (eds.) *Ground-based and Airborne Instrumentation for Astronomy VIII*, vol. 11447, 337 – 350, DOI: [10.1117/12.2561046](https://doi.org/10.1117/12.2561046). International Society for Optics and Photonics (SPIE, 2020).
51. Brogi, M. *et al.* Rotation and Winds of Exoplanet HD 189733 b Measured with High-dispersion Transmission Spectroscopy. *ApJ* **817**, 106, DOI: [10.3847/0004-637X/817/2/106](https://doi.org/10.3847/0004-637X/817/2/106) (2016). [1512.05175](https://arxiv.org/abs/1512.05175).
52. Snellen, I. A. G., de Kok, R. J., de Mooij, E. J. W. & Albrecht, S. The orbital motion, absolute mass and high-altitude winds of exoplanet HD209458b. *Nature* **465**, 1049–1051, DOI: [10.1038/nature09111](https://doi.org/10.1038/nature09111) (2010). [1006.4364](https://arxiv.org/abs/1006.4364).
53. Nugroho, S. K. *et al.* High-resolution Spectroscopic Detection of TiO and a Stratosphere in the Day-side of WASP-33b. *AJ* **154**, 221, DOI: [10.3847/1538-3881/aa9433](https://doi.org/10.3847/1538-3881/aa9433) (2017). [1710.05276](https://arxiv.org/abs/1710.05276).
54. Yan, F. & Henning, T. An extended hydrogen envelope of the extremely hot giant exoplanet KELT-9b. *Nat. Astron.* **2**, 714–718, DOI: [10.1038/s41550-018-0503-3](https://doi.org/10.1038/s41550-018-0503-3) (2018). [1807.00869](https://arxiv.org/abs/1807.00869).
55. Brogi, M. *et al.* The signature of orbital motion from the dayside of the planet τ Boötis b. *Nature* **486**, 502–504, DOI: [10.1038/nature11161](https://doi.org/10.1038/nature11161) (2012). [1206.6109](https://arxiv.org/abs/1206.6109).
56. Snellen, I. High-dispersion spectroscopy of extrasolar planets: from co in hot jupiters to o₂ in exo-earths. *Philos. Transactions Royal Soc. A: Math. Phys. Eng. Sci.* **372**, 20130075, DOI: [10.1098/rsta.2013.0075](https://doi.org/10.1098/rsta.2013.0075) (2014). <https://royalsocietypublishing.org/doi/pdf/10.1098/rsta.2013.0075>.
57. Giacobbe, P. *et al.* Five carbon- and nitrogen-bearing species in a hot giant planet's atmosphere. *Nature* **592**, 205–208, DOI: [10.1038/s41586-021-03381-x](https://doi.org/10.1038/s41586-021-03381-x) (2021). [2104.03352](https://arxiv.org/abs/2104.03352).
58. Merritt, S. R. *et al.* An inventory of atomic species in the atmosphere of WASP-121b using UVES high-resolution spectroscopy. *MNRAS* **506**, 3853–3871, DOI: [10.1093/mnras/stab1878](https://doi.org/10.1093/mnras/stab1878) (2021). [2106.15394](https://arxiv.org/abs/2106.15394).

59. Bello-Arufe, Aaron *et al.* Exoplanet atmospheres at high resolution through a modest-size telescope - fein mascara-2b and kelt-9b with flies on the nordic optical telescope. *A&A* **662**, A51, DOI: [10.1051/0004-6361/202142787](https://doi.org/10.1051/0004-6361/202142787) (2022).
60. Mollière, P. & Snellen, I. A. G. Detecting isotopologues in exoplanet atmospheres using ground-based high-dispersion spectroscopy. *Astron. & Astrophys.* **622**, A139, DOI: [10.1051/0004-6361/201834169](https://doi.org/10.1051/0004-6361/201834169) (2019).
61. Line, M. R. *et al.* A solar C/O and sub-solar metallicity in a hot Jupiter atmosphere. *Nature* **598**, 580–584, DOI: [10.1038/s41586-021-03912-6](https://doi.org/10.1038/s41586-021-03912-6) (2021). [2110.14821](https://doi.org/10.1038/s41586-021-03912-6).
62. Konopacky, Q. M., Barman, T. S., Macintosh, B. A. & Marois, C. Detection of carbon monoxide and water absorption lines in an exoplanet atmosphere. *Science* **339**, 1398–1401, DOI: [10.1126/science.1232003](https://doi.org/10.1126/science.1232003) (2013).
63. Meadows, V. S. *et al.* Exoplanet Biosignatures: Understanding Oxygen as a Biosignature in the Context of Its Environment. *Astrobiology* **18**, 630–662, DOI: [10.1089/ast.2017.1727](https://doi.org/10.1089/ast.2017.1727) (2018). [1705.07560](https://doi.org/10.1089/ast.2017.1727).
64. Brogi, M. *et al.* Detection of Molecular Absorption in the Dayside of Exoplanet 51 Pegasi b? *ApJ* **767**, 27, DOI: [10.1088/0004-637X/767/1/27](https://doi.org/10.1088/0004-637X/767/1/27) (2013). [1302.6242](https://doi.org/10.1088/0004-637X/767/1/27).
65. Brogi, M., de Kok, R. J., Birkby, J. L., Schwarz, H. & Snellen, I. A. G. Carbon monoxide and water vapor in the atmosphere of the non-transiting exoplanet HD 179949 b. *Astronomy and Astrophysics* **565**, A124, DOI: [10.1051/0004-6361/201423537](https://doi.org/10.1051/0004-6361/201423537) (2014). [1404.3769](https://doi.org/10.1051/0004-6361/201423537).
66. Cabot, S. H. C., Madhusudhan, N., Hawker, G. A. & Gandhi, S. On the robustness of analysis techniques for molecular detections using high-resolution exoplanet spectroscopy. *MNRAS* **482**, 4422–4436, DOI: [10.1093/mnras/sty2994](https://doi.org/10.1093/mnras/sty2994) (2019). [1811.05978](https://doi.org/10.1093/mnras/sty2994).
67. de Kok, R. J. *et al.* Detection of carbon monoxide in the high-resolution day-side spectrum of the exoplanet HD 189733b. *Astronomy and Astrophysics* **554**, A82, DOI: [10.1051/0004-6361/201321381](https://doi.org/10.1051/0004-6361/201321381) (2013). [1304.4014](https://doi.org/10.1051/0004-6361/201321381).
68. Rodler, F., Kürster, M. & Barnes, J. R. Detection of CO absorption in the atmosphere of the hot Jupiter HD 189733b. *MNRAS* **432**, 1980–1988, DOI: [10.1093/mnras/stt462](https://doi.org/10.1093/mnras/stt462) (2013).
69. Alonso-Floriano, F. J. *et al.* Multiple water band detections in the CARMENES near-infrared transmission spectrum of HD 189733 b. *Astronomy and Astrophysics* **621**, A74, DOI: [10.1051/0004-6361/201834339](https://doi.org/10.1051/0004-6361/201834339) (2019). [1811.08901](https://doi.org/10.1051/0004-6361/201834339).
70. Birkby, J. L. *et al.* Detection of water absorption in the day side atmosphere of HD 189733 b using ground-based high-resolution spectroscopy at 3.2 μ m. *MNRAS* **436**, L35–L39, DOI: [10.1093/mnras/slt107](https://doi.org/10.1093/mnras/slt107) (2013). [1307.1133](https://doi.org/10.1093/mnras/slt107).
71. Guilluy, G. *et al.* Exoplanet atmospheres with GIANO. II. Detection of molecular absorption in the dayside spectrum of HD 102195b. *Astronomy and Astrophysics* **625**, A107, DOI: [10.1051/0004-6361/201834615](https://doi.org/10.1051/0004-6361/201834615) (2019). [1904.04170](https://doi.org/10.1051/0004-6361/201834615).
72. Hawker, G. A., Madhusudhan, N., Cabot, S. H. C. & Gandhi, S. Evidence for Multiple Molecular Species in the Hot Jupiter HD 209458b. *ApJL* **863**, L11, DOI: [10.3847/2041-8213/aac49d](https://doi.org/10.3847/2041-8213/aac49d) (2018). [1808.03645](https://doi.org/10.3847/2041-8213/aac49d).
73. Lockwood, A. C. *et al.* Near-IR Direct Detection of Water Vapor in Tau Boötis b. *ApJL* **783**, L29, DOI: [10.1088/2041-8205/783/2/L29](https://doi.org/10.1088/2041-8205/783/2/L29) (2014). [1402.0846](https://doi.org/10.1088/2041-8205/783/2/L29).
74. Hoeijmakers, H. J. *et al.* A search for tio in the optical high-resolution transmission spectrum of hd 209458b: Hindrance due to inaccuracies in the line database. *Astron. & Astrophys.* **575**, A20, DOI: [10.1051/0004-6361/201424794](https://doi.org/10.1051/0004-6361/201424794) (2015).
75. Xue, Q. *et al.* JWST Transmission Spectroscopy of HD 209458b: A Supersolar Metallicity, a Very Low C/O, and No Evidence of CH₄, HCN, or C₂H₂. *ApJL* **963**, L5, DOI: [10.3847/2041-8213/ad2682](https://doi.org/10.3847/2041-8213/ad2682) (2024). [2310.03245](https://doi.org/10.3847/2041-8213/ad2682).
76. Kreidberg, L. *et al.* Clouds in the atmosphere of the super-Earth exoplanet GJ1214b. *Nature* **505**, 69–72, DOI: [10.1038/nature12888](https://doi.org/10.1038/nature12888) (2014). [1401.0022](https://doi.org/10.1038/nature12888).
77. Hood, C. E. *et al.* Prospects for Characterizing the Hazeiest Sub-Neptune Exoplanets with High-resolution Spectroscopy. *AJ* **160**, 198, DOI: [10.3847/1538-3881/abb46b](https://doi.org/10.3847/1538-3881/abb46b) (2020). [2008.11299](https://doi.org/10.3847/1538-3881/abb46b).
78. Helling, C. Exoplanet clouds. *Annu. Rev. Earth Planet. Sci.* **47**, 583–606, DOI: [10.1146/annurev-earth-053018-060401](https://doi.org/10.1146/annurev-earth-053018-060401) (2019).
79. Helling, C. *et al.* Exoplanet weather and climate regimes with clouds and thermal ionospheres. A model grid study in support of large-scale observational campaigns. *Astronomy and Astrophysics* **671**, A122, DOI: [10.1051/0004-6361/202243956](https://doi.org/10.1051/0004-6361/202243956) (2023). [2208.05562](https://doi.org/10.1051/0004-6361/202243956).
80. Gandhi, S., Brogi, M. & Webb, R. K. Seeing above the clouds with high-resolution spectroscopy. *MNRAS* **498**, 194–204, DOI: [10.1093/mnras/staa2424](https://doi.org/10.1093/mnras/staa2424) (2020). [2008.11464](https://doi.org/10.1093/mnras/staa2424).
81. Xuan, J. W. *et al.* A clear view of a cloudy brown dwarf companion from high-resolution spectroscopy. *The Astrophys. J.* **937**, 54, DOI: [10.3847/1538-4357/ac8673](https://doi.org/10.3847/1538-4357/ac8673) (2022).
82. Keles, E. *et al.* The PEPsi exoplanet transit survey (PETS) I: investigating the presence of a silicate atmosphere on the super-earth 55 Cnc e. *MNRAS* **513**, 1544–1556, DOI: [10.1093/mnras/stac810](https://doi.org/10.1093/mnras/stac810) (2022). [2203.16856](https://doi.org/10.1093/mnras/stac810).
83. Crossfield, I. J. M., Barman, T. & Hansen, B. M. S. High-resolution, Differential, Near-infrared Transmission Spectroscopy of GJ 1214b. *ApJ* **736**, 132, DOI: [10.1088/0004-637X/736/2/132](https://doi.org/10.1088/0004-637X/736/2/132) (2011). [1104.1173](https://doi.org/10.1088/0004-637X/736/2/132).
84. Esteves, L. J., de Mooij, E. J. W., Jayawardhana, R., Watson, C. & de Kok, R. A Search for Water in a Super-Earth Atmosphere: High-resolution Optical Spectroscopy of 55Cnc e. *AJ* **153**, 268, DOI: [10.3847/1538-3881/aa7133](https://doi.org/10.3847/1538-3881/aa7133) (2017). [1705.03022](https://doi.org/10.3847/1538-3881/aa7133).

85. Goldsmith, P. F. *et al.* O₂ in Interstellar Molecular Clouds. *ApJL* **539**, L123–L127, DOI: [10.1086/312854](https://doi.org/10.1086/312854) (2000).
86. Liseau, R. *et al.* Multi-line detection of O₂ toward ρ Ophiuchi A. *Astronomy and Astrophysics* **541**, A73, DOI: [10.1051/0004-6361/201118575](https://doi.org/10.1051/0004-6361/201118575) (2012). [1202.5637](#).
87. Goldsmith, P. F. *et al.* Herschel Measurements of Molecular Oxygen in Orion. *ApJ* **737**, 96, DOI: [10.1088/0004-637X/737/2/96](https://doi.org/10.1088/0004-637X/737/2/96) (2011). [1108.0441](#).
88. Wang, J. *et al.* Molecular oxygen in the nearest qso mrk 231. *The Astrophys. J.* **889**, 129, DOI: [10.3847/1538-4357/ab612d](https://doi.org/10.3847/1538-4357/ab612d) (2020).
89. Leger, A., Pirre, M. & Marceau, F. J. Search for primitive life on a distant planet: relevance of O₂ and O₃ detections. *Astronomy and Astrophysics* **277**, 309 (1993).
90. Des Marais, D. J. *et al.* Remote Sensing of Planetary Properties and Biosignatures on Extrasolar Terrestrial Planets. *Astrobiology* **2**, 153–181, DOI: [10.1089/15311070260192246](https://doi.org/10.1089/15311070260192246) (2002).
91. Segura, A. *et al.* Ozone Concentrations and Ultraviolet Fluxes on Earth-Like Planets Around Other Stars. *Astrobiology* **3**, 689–708, DOI: [10.1089/15311070322736024](https://doi.org/10.1089/15311070322736024) (2003).
92. Kozakis, T., Mendonça, J. M. & Buchhave, L. A. Is ozone a reliable proxy for molecular oxygen?. I. The O₂-O₃ relationship for Earth-like atmospheres. *Astronomy and Astrophysics* **665**, A156, DOI: [10.1051/0004-6361/202244164](https://doi.org/10.1051/0004-6361/202244164) (2022). [2208.09415](#).
93. Hardegree-Ullman, K. K., Apai, D., Bergsten, G. J., Pascucci, I. & López-Morales, M. Bioverse: A Comprehensive Assessment of the Capabilities of Extremely Large Telescopes to Probe Earth-like O₂ Levels in Nearby Transiting Habitable-zone Exoplanets. *AJ* **165**, 267, DOI: [10.3847/1538-3881/acd1ec](https://doi.org/10.3847/1538-3881/acd1ec) (2023). [2304.12490](#).
94. Clery, D. Future nasa scope would find life on alien worlds. (2023).
95. of Sciences Engineering, N. A. & Medicine. *Exoplanet Science Strategy* (The National Academies Press, Washington, DC, 2018).
96. McLean, I. S. *et al.* Design and development of NIRSPEC: a near-infrared echelle spectrograph for the Keck II telescope. In Fowler, A. M. (ed.) *Infrared Astronomical Instrumentation*, vol. 3354 of *Society of Photo-Optical Instrumentation Engineers (SPIE) Conference Series*, 566–578, DOI: [10.1117/12.317283](https://doi.org/10.1117/12.317283) (1998).
97. Dekker, H., D’Odorico, S., Kaufer, A., Delabre, B. & Kotzlowski, H. Design, construction, and performance of UVES, the echelle spectrograph for the UT2 Kueyen Telescope at the ESO Paranal Observatory. In Iye, M. & Moorwood, A. F. (eds.) *Optical and IR Telescope Instrumentation and Detectors*, vol. 4008 of *Society of Photo-Optical Instrumentation Engineers (SPIE) Conference Series*, 534–545, DOI: [10.1117/12.395512](https://doi.org/10.1117/12.395512) (2000).
98. Noguchi, K. *et al.* High Dispersion Spectrograph (HDS) for the Subaru Telescope. *PASJ* **54**, 855–864, DOI: [10.1093/pasj/54.6.855](https://doi.org/10.1093/pasj/54.6.855) (2002).
99. Kotani, T. *et al.* The infrared Doppler (IRD) instrument for the Subaru telescope: instrument description and commissioning results. In Evans, C. J., Simard, L. & Takami, H. (eds.) *Ground-based and Airborne Instrumentation for Astronomy VII*, vol. 10702 of *Society of Photo-Optical Instrumentation Engineers (SPIE) Conference Series*, 1070211, DOI: [10.1117/12.2311836](https://doi.org/10.1117/12.2311836) (2018).
100. Moutou, C. *et al.* SPIRou: a spectropolarimeter for the CFHT. In *SF2A-2015: Proceedings of the Annual meeting of the French Society of Astronomy and Astrophysics*, 205–212, DOI: [10.48550/arXiv.1510.01368](https://doi.org/10.48550/arXiv.1510.01368) (2015). [1510.01368](#).
101. Kaeufl, H.-U. *et al.* CRIRES: a high-resolution infrared spectrograph for ESO’s VLT. In Moorwood, A. F. M. & Iye, M. (eds.) *Ground-based Instrumentation for Astronomy*, vol. 5492 of *Society of Photo-Optical Instrumentation Engineers (SPIE) Conference Series*, 1218–1227, DOI: [10.1117/12.551480](https://doi.org/10.1117/12.551480) (2004).
102. Dorn, R. J. *et al.* CRIRES⁺ on sky at the ESO Very Large Telescope. Observing the Universe at infrared wavelengths and high spectral resolution. *Astronomy and Astrophysics* **671**, A24, DOI: [10.1051/0004-6361/202245217](https://doi.org/10.1051/0004-6361/202245217) (2023).
103. Oliva, E. *et al.* GIANO, the high resolution IR spectrograph of the TNG: geometry of the echellogram and strategies for the 2D reduction of the spectra. In Evans, C. J., Simard, L. & Takami, H. (eds.) *Ground-based and Airborne Instrumentation for Astronomy VII*, vol. 10702 of *Society of Photo-Optical Instrumentation Engineers (SPIE) Conference Series*, 1070274, DOI: [10.1117/12.2309927](https://doi.org/10.1117/12.2309927) (2018).
104. Quirrenbach, A. *et al.* CARMENES instrument overview. In *Ground-based and Airborne Instrumentation for Astronomy V*, vol. 9147 of *Proc. SPIE*, 91471F, DOI: [10.1117/12.2056453](https://doi.org/10.1117/12.2056453) (2014).
105. Park, C. *et al.* Design and early performance of IGRINS (Immersion Grating Infrared Spectrometer). In Ramsay, S. K., McLean, I. S. & Takami, H. (eds.) *Ground-based and Airborne Instrumentation for Astronomy V*, vol. 9147 of *Society of Photo-Optical Instrumentation Engineers (SPIE) Conference Series*, 91471D, DOI: [10.1117/12.2056431](https://doi.org/10.1117/12.2056431) (2014).
106. Mayor, M. *et al.* Setting New Standards with HARPS. *The Messenger* **114**, 20–24 (2003).
107. Cosentino, R. *et al.* Harps-N: the new planet hunter at TNG. In McLean, I. S., Ramsay, S. K. & Takami, H. (eds.) *Ground-based and Airborne Instrumentation for Astronomy IV*, vol. 8446 of *Society of Photo-Optical Instrumentation Engineers (SPIE) Conference Series*, 84461V, DOI: [10.1117/12.925738](https://doi.org/10.1117/12.925738) (2012).
108. Cale, B. L. *et al.* Commissioning observations of HD 189733 with the Palomar Radial Velocity Instrument. *J. Astron. Telesc. Instruments, Syst.* **9**, 038006, DOI: [10.1117/1.JATIS.9.3.038006](https://doi.org/10.1117/1.JATIS.9.3.038006) (2023).

109. Blackman, R. T. *et al.* Performance Verification of the EXtreme PREcision Spectrograph. *AJ* **159**, 238, DOI: [10.3847/1538-3881/ab811d](https://doi.org/10.3847/1538-3881/ab811d) (2020). [2003.08852](https://arxiv.org/abs/2003.08852).
110. Wildi, F. *et al.* First light of NIRPS, the near-infrared adaptive-optics assisted high resolution spectrograph for the ESO 3.6m. In Evans, C. J., Bryant, J. J. & Motohara, K. (eds.) *Ground-based and Airborne Instrumentation for Astronomy IX*, vol. 12184 of *Society of Photo-Optical Instrumentation Engineers (SPIE) Conference Series*, 121841H, DOI: [10.1117/12.2630016](https://doi.org/10.1117/12.2630016) (2022).
111. Crass, J. *et al.* The final design of the iLocater spectrograph: an optimized architecture for diffraction-limited EPRV instruments. In Evans, C. J., Bryant, J. J. & Motohara, K. (eds.) *Ground-based and Airborne Instrumentation for Astronomy IX*, vol. 12184 of *Society of Photo-Optical Instrumentation Engineers (SPIE) Conference Series*, 121841P, DOI: [10.1117/12.2630228](https://doi.org/10.1117/12.2630228) (2022). [2209.00009](https://arxiv.org/abs/2209.00009).
112. Bechter, A. J., Bechter, E. B., Crepp, J. R., King, D. & Crass, J. A radial velocity error budget for single-mode Doppler spectrographs. In Evans, C. J., Simard, L. & Takami, H. (eds.) *Ground-based and Airborne Instrumentation for Astronomy VII*, vol. 10702 of *Society of Photo-Optical Instrumentation Engineers (SPIE) Conference Series*, 107026T, DOI: [10.1117/12.2313658](https://doi.org/10.1117/12.2313658) (2018). [1812.02704](https://arxiv.org/abs/1812.02704).
113. Pepe, F. *et al.* ESPRESSO at VLT. On-sky performance and first results. *Astronomy and Astrophysics* **645**, A96, DOI: [10.1051/0004-6361/202038306](https://doi.org/10.1051/0004-6361/202038306) (2021). [2010.00316](https://arxiv.org/abs/2010.00316).
114. Strassmeier, K. G. *et al.* PEPsi: The high-resolution échelle spectrograph and polarimeter for the Large Binocular Telescope. *Astron. Nachrichten* **336**, 324, DOI: [10.1002/asna.201512172](https://doi.org/10.1002/asna.201512172) (2015). [1505.06492](https://arxiv.org/abs/1505.06492).
115. Kuo Tiong, B. C. *et al.* IRANTI: a compact flexible configuration infrared échelle spectrograph integrating emerging technologies for precise radial velocity measurements. In Evans, C. J., Bryant, J. J. & Motohara, K. (eds.) *Ground-based and Airborne Instrumentation for Astronomy VIII*, vol. 11447 of *Society of Photo-Optical Instrumentation Engineers (SPIE) Conference Series*, 114474H, DOI: [10.1117/12.2561352](https://doi.org/10.1117/12.2561352) (2020).
116. Schroeder, D. J. *Astronomical Optics* (Elsevier, 2000).
117. Crepp, J. R. Improving planet-finding spectrometers. *Science* **346**, 809–810, DOI: [10.1126/science.1262071](https://doi.org/10.1126/science.1262071) (2014). [1412.2992](https://arxiv.org/abs/1412.2992).
118. Jovanovic, N. *et al.* Efficiently feeding single-mode fiber photonic spectrographs with an extreme adaptive optics system: on-sky characterization and preliminary spectroscopy. In Evans, C. J., Simard, L. & Takami, H. (eds.) *Ground-based and Airborne Instrumentation for Astronomy VI*, vol. 9908 of *Society of Photo-Optical Instrumentation Engineers (SPIE) Conference Series*, 99080R, DOI: [10.1117/12.2234299](https://doi.org/10.1117/12.2234299) (2016).
119. El Morsy, M. *et al.* Validation of strategies for coupling exoplanet psfs into single-mode fibres for high-dispersion coronagraphy. *Astron. & Astrophys.* **667**, A171, DOI: [10.1051/0004-6361/202243408](https://doi.org/10.1051/0004-6361/202243408) (2022).
120. Shaklan, S. & Roddier, F. Coupling starlight into single-mode fiber optics. *Appl. Opt.* **27**, 2334–2338, DOI: [10.1364/AO.27.002334](https://doi.org/10.1364/AO.27.002334) (1988).
121. Jovanovic, N. *et al.* Efficient injection from large telescopes into single-mode fibres: Enabling the era of ultra-precision astronomy. *Astronomy and Astrophysics* **604**, A122, DOI: [10.1051/0004-6361/201630351](https://doi.org/10.1051/0004-6361/201630351) (2017). [1706.08821](https://arxiv.org/abs/1706.08821).
122. Otten, G. P. P. L. *et al.* Direct characterization of young giant exoplanets at high spectral resolution by coupling SPHERE and CRiES+. *Astronomy and Astrophysics* **646**, A150, DOI: [10.1051/0004-6361/202038517](https://doi.org/10.1051/0004-6361/202038517) (2021). [2009.01841](https://arxiv.org/abs/2009.01841).
123. Davis, S. P., Abrams, M. C. & Brault, J. W. *Fourier transform spectrometry* (Elsevier, 2001).
124. Hall, D. N. B., Ridgway, S., Bell, E. A. & Yarborough, J. M. A 1.4 Meter Fourier Transform Spectrometer for Astronomical Observations. In Crawford, D. L. (ed.) *Instrumentation in Astronomy III*, vol. 172 of *Society of Photo-Optical Instrumentation Engineers (SPIE) Conference Series*, 121, DOI: [10.1117/12.957074](https://doi.org/10.1117/12.957074) (1979).
125. Behr, B. B. *et al.* Stellar Astrophysics with a Dispersed Fourier Transform Spectrograph. I. Instrument Description and Orbits of Single-lined Spectroscopic Binaries. *ApJ* **705**, 543–553, DOI: [10.1088/0004-637X/705/1/543](https://doi.org/10.1088/0004-637X/705/1/543) (2009). [0909.3241](https://arxiv.org/abs/0909.3241).
126. Wallace, L., Hinkle, K. H., Livingston, W. C. & Davis, S. P. An Optical and Near-infrared (2958–9250 Å) Solar Flux Atlas. *ApJS* **195**, 6, DOI: [10.1088/0067-0049/195/1/6](https://doi.org/10.1088/0067-0049/195/1/6) (2011).
127. Reiners, A., Mrotzek, N., Lemke, U., Hinrichs, J. & Reinsch, K. The IAG solar flux atlas: Accurate wavelengths and absolute convective blueshift in standard solar spectra. *Astronomy and Astrophysics* **587**, A65, DOI: [10.1051/0004-6361/201527530](https://doi.org/10.1051/0004-6361/201527530) (2016). [1511.03014](https://arxiv.org/abs/1511.03014).
128. Shirasaki, M. Virtually imaged phased array. *Fujitsu Sci. & Tech. J.* **35**, 113–125 (1999).
129. Zhu, X., Lin, D., Hao, Z., Wang, L. & He, J. A VIPA spectrograph with ultra-high resolution and wavelength calibration for astronomical applications. *The Astron. J.* **160**, 135, DOI: [10.3847/1538-3881/aba836](https://doi.org/10.3847/1538-3881/aba836) (2020).
130. Bourdarot, G. *et al.* Nanovipa: a miniaturized high-resolution echelle spectrometer, for the monitoring of young stars from a 6u cubesat. *CEAS Space J.* **9**, 411–419 (2017).
131. Zhu, X., Lin, D., Zhang, Z., Xie, X. & He, J. Dispersion Characteristics of the Multi-mode Fiber-fed VIPA Spectrograph. *AJ* **165**, 228, DOI: [10.3847/1538-3881/accc30](https://doi.org/10.3847/1538-3881/accc30) (2023).
132. Carlotti, A. *et al.* On-sky demonstration at Palomar Observatory of the near-IR, high-resolution VIPA spectrometer. In Evans, C. J., Bryant, J. J. & Motohara, K. (eds.) *Ground-based and Airborne Instrumentation for Astronomy IX*, vol. 12184 of *Society of Photo-Optical Instrumentation Engineers (SPIE) Conference Series*, 121841I, DOI: [10.1117/12.2628937](https://doi.org/10.1117/12.2628937) (2022). [2305.19736](https://arxiv.org/abs/2305.19736).

133. Rukdee, S. *et al.* First on-sky results of a Fabry-Perot Instrument for Oxygen Searches (FIOS) prototype. *Astronomy and Astrophysics* **678**, A114, DOI: [10.1051/0004-6361/202346619](https://doi.org/10.1051/0004-6361/202346619) (2023). [2307.14947](https://arxiv.org/abs/2307.14947).
134. Fowler, J. *et al.* Visible extreme adaptive optics on extremely large telescopes: Towards detecting oxygen in Proxima Centauri b and analogs. *arXiv e-prints* arXiv:2309.00725, DOI: [10.48550/arXiv.2309.00725](https://doi.org/10.48550/arXiv.2309.00725) (2023). [2309.00725](https://arxiv.org/abs/2309.00725).
135. Le, H. A. N. *et al.* Exposure time calculator for Immersion Grating Infrared Spectrograph: IGRINS. *Adv. Space Res.* **55**, 2509–2518, DOI: [10.1016/j.asr.2015.03.007](https://doi.org/10.1016/j.asr.2015.03.007) (2015). [1501.03249](https://arxiv.org/abs/1501.03249).
136. Rukdee, S. *et al.* Tardys: Design and prototype of an exoplanet hunter for tao using a r6 echelle grating. *Exp. Astron.* **48**, 145–169, DOI: [10.1007/s10686-019-09642-y](https://doi.org/10.1007/s10686-019-09642-y) (2019).
137. Vanzi, L. *et al.* Precision stellar radial velocity measurements with FIDEOS at the ESO 1-m telescope of La Silla. *MNRAS* **477**, 5041–5051, DOI: [10.1093/mnras/sty936](https://doi.org/10.1093/mnras/sty936) (2018). [1804.07441](https://arxiv.org/abs/1804.07441).
138. Noll, S. *et al.* An atmospheric radiation model for Cerro Paranal. I. The optical spectral range. *Astronomy and Astrophysics* **543**, A92, DOI: [10.1051/0004-6361/201219040](https://doi.org/10.1051/0004-6361/201219040) (2012). [1205.2003](https://arxiv.org/abs/1205.2003).
139. Jones, A., Noll, S., Kausch, W., Szyszka, C. & Kimeswenger, S. An advanced scattered moonlight model for Cerro Paranal. *Astronomy and Astrophysics* **560**, A91, DOI: [10.1051/0004-6361/201322433](https://doi.org/10.1051/0004-6361/201322433) (2013). [1310.7030](https://arxiv.org/abs/1310.7030).
140. Moehler, S. *et al.* Flux calibration of medium-resolution spectra from 300 nm to 2500 nm: Model reference spectra and telluric correction. *Astronomy and Astrophysics* **568**, A9, DOI: [10.1051/0004-6361/201423790](https://doi.org/10.1051/0004-6361/201423790) (2014). [1408.1797](https://arxiv.org/abs/1408.1797).
141. Vernet, J. *et al.* X-shooter, the new wide band intermediate resolution spectrograph at the eso very large telescope. *Astron. & Astrophys.* **536**, A105, DOI: [10.1051/0004-6361/201117752](https://doi.org/10.1051/0004-6361/201117752) (2011).
142. Tsiaras, A. *et al.* A Population Study of Gaseous Exoplanets. *AJ* **155**, 156, DOI: [10.3847/1538-3881/aaaf75](https://doi.org/10.3847/1538-3881/aaaf75) (2018). [1704.05413](https://arxiv.org/abs/1704.05413).
143. Tsiaras, A., Waldmann, I. P., Tinetti, G., Tennyson, J. & Yurchenko, S. N. Water vapour in the atmosphere of the habitable-zone eight-Earth-mass planet K2-18 b. *Nat. Astron.* **3**, 1086–1091, DOI: [10.1038/s41550-019-0878-9](https://doi.org/10.1038/s41550-019-0878-9) (2019). [1909.05218](https://arxiv.org/abs/1909.05218).
144. Edwards, B. *et al.* Characterizing a World Within the Hot-Neptune Desert: Transit Observations of LTT 9779 b with the Hubble Space Telescope/WFC3. *AJ* **166**, 158, DOI: [10.3847/1538-3881/acea77](https://doi.org/10.3847/1538-3881/acea77) (2023). [2306.13645](https://arxiv.org/abs/2306.13645).
145. Kreidberg, L. *et al.* Tentative Evidence for Water Vapor in the Atmosphere of the Neptune-sized Exoplanet HD 106315c. *AJ* **164**, 124, DOI: [10.3847/1538-3881/ac85be](https://doi.org/10.3847/1538-3881/ac85be) (2022). [2006.07444](https://arxiv.org/abs/2006.07444).
146. Mikal-Evans, T. *et al.* Hubble Space Telescope Transmission Spectroscopy for the Temperate Sub-Neptune TOI-270 d: A Possible Hydrogen-rich Atmosphere Containing Water Vapor. *AJ* **165**, 84, DOI: [10.3847/1538-3881/aca90b](https://doi.org/10.3847/1538-3881/aca90b) (2023). [2211.15576](https://arxiv.org/abs/2211.15576).
147. Roy, P.-A. *et al.* Water Absorption in the Transmission Spectrum of the Water World Candidate GJ 9827 d. *ApJL* **954**, L52, DOI: [10.3847/2041-8213/acebf0](https://doi.org/10.3847/2041-8213/acebf0) (2023). [2309.10845](https://arxiv.org/abs/2309.10845).
148. Edwards, B. *et al.* Hubble WFC3 Spectroscopy of the Habitable-zone Super-Earth LHS 1140 b. *AJ* **161**, 44, DOI: [10.3847/1538-3881/abc6a5](https://doi.org/10.3847/1538-3881/abc6a5) (2021). [2011.08815](https://arxiv.org/abs/2011.08815).
149. Brande, J. *et al.* A Mirage or an Oasis? Water Vapor in the Atmosphere of the Warm Neptune TOI-674 b. *AJ* **164**, 197, DOI: [10.3847/1538-3881/ac8b7e](https://doi.org/10.3847/1538-3881/ac8b7e) (2022). [2201.04197](https://arxiv.org/abs/2201.04197).
150. Bean, J. L. *et al.* High atmospheric metal enrichment for a Saturn-mass planet. *Nature* **618**, 43–46, DOI: [10.1038/s41586-023-05984-y](https://doi.org/10.1038/s41586-023-05984-y) (2023). [2303.14206](https://arxiv.org/abs/2303.14206).
151. Swain, M. R. *et al.* Detection of an Atmosphere on a Rocky Exoplanet. *AJ* **161**, 213, DOI: [10.3847/1538-3881/abe879](https://doi.org/10.3847/1538-3881/abe879) (2021). [2103.05657](https://arxiv.org/abs/2103.05657).
152. Madhusudhan, N. *et al.* Carbon-bearing Molecules in a Possible Hycean Atmosphere. *ApJL* **956**, L13, DOI: [10.3847/2041-8213/acf577](https://doi.org/10.3847/2041-8213/acf577) (2023). [2309.05566](https://arxiv.org/abs/2309.05566).
153. Tsiaras, A. *et al.* Detection of an Atmosphere Around the Super-Earth 55 Cancri e. *ApJ* **820**, 99, DOI: [10.3847/0004-637X/820/2/99](https://doi.org/10.3847/0004-637X/820/2/99) (2016). [1511.08901](https://arxiv.org/abs/1511.08901).
154. Brogi, M., Line, M., Bean, J., Désert, J.-M. & Schwarz, H. A framework to combine low- and high-resolution spectroscopy for the atmospheres of transiting exoplanets. *The Astrophys. J.* **839**, L2, DOI: [10.3847/2041-8213/aa6933](https://doi.org/10.3847/2041-8213/aa6933) (2017).
155. Pino, L. *et al.* Combining low- to high-resolution transit spectroscopy of HD 189733b. Linking the troposphere and the thermosphere of a hot gas giant. *Astronomy and Astrophysics* **612**, A53, DOI: [10.1051/0004-6361/201731244](https://doi.org/10.1051/0004-6361/201731244) (2018). [1709.09678](https://arxiv.org/abs/1709.09678).
156. Dressel, L. & Marinelli, M. Wide field camera 3 instrument handbook, version 15. *Balt. STScI* (2023).
157. Fleming, B. T. *et al.* Colorado Ultraviolet Transit Experiment: a dedicated CubeSat mission to study exoplanetary mass loss and magnetic fields. *J. Astron. Telesc. Instruments, Syst.* **4**, 014004, DOI: [10.1117/1.JATIS.4.1.014004](https://doi.org/10.1117/1.JATIS.4.1.014004) (2018). [1801.02673](https://arxiv.org/abs/1801.02673).
158. Tinetti, G. *et al.* The science of ARIEL (Atmospheric Remote-sensing Infrared Exoplanet Large-survey). In MacEwen, H. A. *et al.* (eds.) *Space Telescopes and Instrumentation 2016: Optical, Infrared, and Millimeter Wave*, vol. 9904 of *Society of Photo-Optical Instrumentation Engineers (SPIE) Conference Series*, 99041X, DOI: [10.1117/12.2232370](https://doi.org/10.1117/12.2232370) (2016).

159. Stotesbury, I. *et al.* Twinkle: a small satellite spectroscopy mission for the next phase of exoplanet science. In Coyle, L. E., Matsuura, S. & Perrin, M. D. (eds.) *Space Telescopes and Instrumentation 2022: Optical, Infrared, and Millimeter Wave*, vol. 12180 of *Society of Photo-Optical Instrumentation Engineers (SPIE) Conference Series*, 1218033, DOI: [10.1117/12.2641373](https://doi.org/10.1117/12.2641373) (2022). [2209.03337](https://arxiv.org/abs/2209.03337).
160. Ricker, G. R. *et al.* Transiting Exoplanet Survey Satellite. *J. Astron. Telesc. Instruments, Syst.* **1**, 1 – 10, DOI: [10.1117/1.JATIS.1.1.014003](https://doi.org/10.1117/1.JATIS.1.1.014003) (2014).
161. Rando, N. *et al.* CHEOPS, the ESA mission for exo-planets characterization: early operations and commissioning results. In Lystrup, M., Perrin, M. D., Batalha, N., Siegler, N. & Tong, E. C. (eds.) *Space Telescopes and Instrumentation 2020: Optical, Infrared, and Millimeter Wave*, vol. 11443, 208 – 221, DOI: [10.1117/12.2567296](https://doi.org/10.1117/12.2567296). International Society for Optics and Photonics (SPIE, 2020).
162. A-thano, N. *et al.* Revisiting the Transit Timing and Atmosphere Characterization of the Neptune-mass Planet HAT-P-26 b. *AJ* **166**, 223, DOI: [10.3847/1538-3881/acfee](https://doi.org/10.3847/1538-3881/acfee) (2023). [2303.03610](https://arxiv.org/abs/2303.03610).
163. Basilicata, M. *et al.* The GAPS Programme at TNG LV. Multiple molecular species in the atmosphere of HAT-P-11 b and review of the HAT-P-11 planetary system. *arXiv e-prints* arXiv:2403.01527, DOI: [10.48550/arXiv.2403.01527](https://doi.org/10.48550/arXiv.2403.01527) (2024). [2403.01527](https://arxiv.org/abs/2403.01527).
164. Radica, M. *et al.* Muted Features in the JWST NIRISS Transmission Spectrum of Hot Neptune LTT 9779b. *ApJL* **962**, L20, DOI: [10.3847/2041-8213/ad20e4](https://doi.org/10.3847/2041-8213/ad20e4) (2024). [2401.15548](https://arxiv.org/abs/2401.15548).
165. Benneke, B. *et al.* JWST Reveals CH₄, CO₂, and H₂O in a Metal-rich Miscible Atmosphere on a Two-Earth-Radius Exoplanet. *arXiv e-prints* arXiv:2403.03325, DOI: [10.48550/arXiv.2403.03325](https://doi.org/10.48550/arXiv.2403.03325) (2024). [2403.03325](https://arxiv.org/abs/2403.03325).
166. Holmberg, M. & Madhusudhan, N. Possible Hycean conditions in the sub-Neptune TOI-270 d. *Astronomy and Astrophysics* **683**, L2, DOI: [10.1051/0004-6361/202348238](https://doi.org/10.1051/0004-6361/202348238) (2024). [2403.03244](https://arxiv.org/abs/2403.03244).
167. Benneke, B. *et al.* Water Vapor and Clouds on the Habitable-zone Sub-Neptune Exoplanet K2-18b. *ApJL* **887**, L14, DOI: [10.3847/2041-8213/ab59dc](https://doi.org/10.3847/2041-8213/ab59dc) (2019). [1909.04642](https://arxiv.org/abs/1909.04642).
168. Damiano, M., Bello-Arufe, A., Yang, J. & Hu, R. LHS 1140 b is a potentially habitable water world. *arXiv e-prints* arXiv:2403.13265, DOI: [10.48550/arXiv.2403.13265](https://doi.org/10.48550/arXiv.2403.13265) (2024). [2403.13265](https://arxiv.org/abs/2403.13265).
169. Greene, T. P. *et al.* Thermal emission from the Earth-sized exoplanet TRAPPIST-1 b using JWST. *Nature* **618**, 39–42, DOI: [10.1038/s41586-023-05951-7](https://doi.org/10.1038/s41586-023-05951-7) (2023). [2303.14849](https://arxiv.org/abs/2303.14849).
170. Lim, O. *et al.* Atmospheric Reconnaissance of TRAPPIST-1 b with JWST/NIRISS: Evidence for Strong Stellar Contamination in the Transmission Spectra. *ApJL* **955**, L22, DOI: [10.3847/2041-8213/acf7c4](https://doi.org/10.3847/2041-8213/acf7c4) (2023). [2309.07047](https://arxiv.org/abs/2309.07047).
171. Bézard, B., Charnay, B. & Blain, D. Methane as a dominant absorber in the habitable-zone sub-Neptune K2-18 b. *arXiv e-prints* arXiv:2011.10424, DOI: [10.48550/arXiv.2011.10424](https://doi.org/10.48550/arXiv.2011.10424) (2020). [2011.10424](https://arxiv.org/abs/2011.10424).
172. Deibert, E. K. *et al.* A Near-infrared Chemical Inventory of the Atmosphere of 55 Cancri e. *AJ* **161**, 209, DOI: [10.3847/1538-3881/abe768](https://doi.org/10.3847/1538-3881/abe768) (2021). [2102.08965](https://arxiv.org/abs/2102.08965).
173. May, E. M. *et al.* Double Trouble: Two Transits of the Super-Earth GJ 1132 b Observed with JWST NIRSpec G395H. *ApJL* **959**, L9, DOI: [10.3847/2041-8213/ad054f](https://doi.org/10.3847/2041-8213/ad054f) (2023). [2310.10711](https://arxiv.org/abs/2310.10711).
174. Mugnai, L. V. *et al.* ARES. V. No Evidence For Molecular Absorption in the HST WFC3 Spectrum of GJ 1132 b. *AJ* **161**, 284, DOI: [10.3847/1538-3881/abf3c3](https://doi.org/10.3847/1538-3881/abf3c3) (2021). [2104.01873](https://arxiv.org/abs/2104.01873).
175. Beatty, T. G. *et al.* Sulfur Dioxide and Other Molecular Species in the Atmosphere of the Sub-Neptune GJ 3470 b. *ApJL* **970**, L10, DOI: [10.3847/2041-8213/ad55e9](https://doi.org/10.3847/2041-8213/ad55e9) (2024). [2406.04450](https://arxiv.org/abs/2406.04450).
176. Grasser, N., Snellen, I. A. G., Landman, R., Picos, D. G. & Gandhi, S. Peering above the clouds of the warm Neptune GJ 436 b with CRIRES+. *Astronomy and Astrophysics* **688**, A191, DOI: [10.1051/0004-6361/202449932](https://doi.org/10.1051/0004-6361/202449932) (2024). [2407.06707](https://arxiv.org/abs/2407.06707).
177. Barclay, T. *et al.* The transmission spectrum of the potentially rocky planet L 98-59 c. *arXiv e-prints* arXiv:2301.10866, DOI: [10.48550/arXiv.2301.10866](https://doi.org/10.48550/arXiv.2301.10866) (2023). [2301.10866](https://arxiv.org/abs/2301.10866).
178. Damiano, M. *et al.* A Transmission Spectrum of the Sub-Earth Planet L98-59 b in 1.1–1.7 μ m. *AJ* **164**, 225, DOI: [10.3847/1538-3881/ac9472](https://doi.org/10.3847/1538-3881/ac9472) (2022). [2210.10008](https://arxiv.org/abs/2210.10008).
179. Zhou, L., Ma, B., Wang, Y. & Zhu, Y. Hubble WFC3 Spectroscopy of the Rocky Planet L 98-59 b: No Evidence for a Cloud-free Primordial Atmosphere. *AJ* **164**, 203, DOI: [10.3847/1538-3881/ac8fe9](https://doi.org/10.3847/1538-3881/ac8fe9) (2022). [2210.10699](https://arxiv.org/abs/2210.10699).
180. Ridden-Harper, A. *et al.* High-resolution Transmission Spectroscopy of the Terrestrial Exoplanet GJ 486b. *AJ* **165**, 170, DOI: [10.3847/1538-3881/acbd39](https://doi.org/10.3847/1538-3881/acbd39) (2023). [2212.11816](https://arxiv.org/abs/2212.11816).
181. Bouwman, J. *et al.* Spectroscopic Time Series Performance of the Mid-infrared Instrument on the JWST. *PASP* **135**, 038002, DOI: [10.1088/1538-3873/acbc49](https://doi.org/10.1088/1538-3873/acbc49) (2023). [2211.16123](https://arxiv.org/abs/2211.16123).
182. Zhang, M. *et al.* GJ 367b Is a Dark, Hot, Airless Sub-Earth. *ApJL* **961**, L44, DOI: [10.3847/2041-8213/ad1a07](https://doi.org/10.3847/2041-8213/ad1a07) (2024). [2401.01400](https://arxiv.org/abs/2401.01400).
183. Diamond-Lowe, H., Mendonça, J. M., Charbonneau, D. & Buchhave, L. A. Ground-based Optical Transmission Spectroscopy of the Nearby Terrestrial Exoplanet LTT 1445Ab. *AJ* **165**, 169, DOI: [10.3847/1538-3881/acbf39](https://doi.org/10.3847/1538-3881/acbf39) (2023). [2210.11809](https://arxiv.org/abs/2210.11809).

184. Garcia, L. J. *et al.* HST/WFC3 transmission spectroscopy of the cold rocky planet TRAPPIST-1h. *Astronomy and Astrophysics* **665**, A19, DOI: [10.1051/0004-6361/202142603](https://doi.org/10.1051/0004-6361/202142603) (2022). [2203.13698](https://arxiv.org/abs/2203.13698).
185. Moran, S. E. *et al.* High Tide or Riptide on the Cosmic Shoreline? A Water-rich Atmosphere or Stellar Contamination for the Warm Super-Earth GJ 486b from JWST Observations. *ApJL* **948**, L11, DOI: [10.3847/2041-8213/accb9c](https://doi.org/10.3847/2041-8213/accb9c) (2023). [2305.00868](https://arxiv.org/abs/2305.00868).
186. López-Morales, M. *et al.* Optimizing Ground-based Observations of O₂ in Earth Analogs. *AJ* **158**, 24, DOI: [10.3847/1538-3881/ab21d7](https://doi.org/10.3847/1538-3881/ab21d7) (2019). [1905.05862](https://arxiv.org/abs/1905.05862).
187. Team, T. L. The luvoir mission concept study final report (2019). [1912.06219](https://arxiv.org/abs/1912.06219).
188. Gaudi, B. S. *et al.* The habitable exoplanet observatory (habex) mission concept study final report (2020). [2001.06683](https://arxiv.org/abs/2001.06683).
189. Tacconi, L. *et al.* Voyage 2050 – Final recommendations from the Voyage 2050 Senior Committee. *Eur. Space Agency* (2021).
190. Plavchan, P. *et al.* EarthFinder Probe Mission Concept Study: Characterizing nearby stellar exoplanet systems with Earth-mass analogs for future direct imaging. *arXiv e-prints* arXiv:2006.13428, DOI: [10.48550/arXiv.2006.13428](https://doi.org/10.48550/arXiv.2006.13428) (2020). [2006.13428](https://arxiv.org/abs/2006.13428).
191. Bourdarot, G. *et al.* Experimental test of a 40 cm-long R=100 000 spectrometer for exoplanet characterisation. In Evans, C. J., Simard, L. & Takami, H. (eds.) *Ground-based and Airborne Instrumentation for Astronomy VII*, vol. 10702 of *Society of Photo-Optical Instrumentation Engineers (SPIE) Conference Series*, 107025Y, DOI: [10.1117/12.2311696](https://doi.org/10.1117/12.2311696) (2018). [1812.09272](https://arxiv.org/abs/1812.09272).
192. Zhang, J., Bottom, M. & Serabyn, E. Direct detection and characterization of exoplanets using imaging Fourier transform spectroscopy. *arXiv e-prints* arXiv:2310.15231, DOI: [10.48550/arXiv.2310.15231](https://doi.org/10.48550/arXiv.2310.15231) (2023). [2310.15231](https://arxiv.org/abs/2310.15231).
193. Atkins, C. *et al.* Lightweighting design optimisation for additively manufactured mirrors. In Hull, T. B., Kim, D. W. & Hallibert, P. (eds.) *Astronomical Optics: Design, Manufacture, and Test of Space and Ground Systems II*, vol. 11116 of *Society of Photo-Optical Instrumentation Engineers (SPIE) Conference Series*, 1111617, DOI: [10.1117/12.2528105](https://doi.org/10.1117/12.2528105) (2019).

Acknowledgements

Author acknowledge the use of the `ExoAtmospheres Database`, `Exoplanet Encyclopedia` and `NASA Exoplanet Archive` database during the preparation of this work. The X-Shooter spectra are based on data obtained from the ESO Science Archive Facility with DOI(s): <https://doi.eso.org/10.18727/archive/71>. S.R. thanks Johannes Buchner for reading the manuscript.

Author contributions statement

S.R. contributed to all aspects of the manuscript.

Additional information

Competing interests

The author declares no competing interests.

Data and code availability

The datasets used and/or analyzed are available from the corresponding author on reasonable request.